NTNU
Norwegian University of
Science and Technology

In silico Investigation of Possible Mitotic Checkpoint Signalling Mechanisms

Håkon Kirkeby

Master of Science in Physics and Mathematics
Submission date: December 2007
Supervisor: Karl Henning Omre, MATH

Norwegian University of Science and Technology
Department of Mathematical Sciences

Problem Description

The objective of the thesis is to construct a quantitative modelling framework for simulation of the mitotic checkpoint "wait-anaphase" signal. This should provide an opportunity to investigate several molecular mechanisms suggested in the literature.

Assignment given: 28. June 2007
Supervisor: Karl Henning Omre, MATH

Foreword

This thesis completes the requirements for course *TMA4900 Matematikk, masteroppgave* and finalizes the Master's programme in Industrial Mathematics at the Norwegian University of Science and Technology (NTNU). The research documented in this thesis was conducted mainly at Harvard Medical School in Boston, USA, as a Pre-doctoral Research Fellow during 2006 and 2007.

First of all, I must express my enormous gratefulness to Professor Jagesh V. Shah at Harvard Medical Shool, for inviting me to his lab and allowing me to use his resources for my thesis work. It has been a true privilege to apply mathematical techniques in a biological setting under these circumstances. I have learned more than I ever expected!

Without the clever ways of my good friend from UKA, Dr. Kristian Wright, I do not think my visit at Harvard would have been possible. Thanks, Kris!

Adviser and mentor at NTNU, Professor Karl Henning Omre, just as much deserve my greetings. Thanks for always supporting me and for being an outstanding pragmatist.

Next, thank you very much Dr. Michael Scott Manak, for sitting next to me in the lab in Boston and for answering all my basic questions about biology. You have been a priceless contribution to my progress and learning, and become a good friend.

Co-supervisor at NTNU, Professor Harald Hanche-Olsen, thanks for making sure that my work stayed more or less in line with the rigours ways of true mathematicians as your self.

On the more personal side, I am in debt to my lovely girlfriend, Ragnhild, for staying with me while I worked in Boston. Thanks also to my parents for keeping me alive, especially when Lånekassen decided not to do that anymore.

Håkon Kirkeby
Nittedal, Dec. 2007

Abstract

The mitotic checkpoint is the major safety mechanism acting to ensure stable genome content in cell division. A delay in chromosome segregation is enforced as long as at least one kinetochore is in lack of proper attachment to the mitotic spindle. In such, no chromosome is left behind or misplaced in mitosis. The attachment state of the chromosomes is monitored by the "wait-anaphase" signal. It is an established model that the formation of an anaphase-inhibiting complex at the unattached kinetochores is the backbone of this signal. However, this model alone can hardly provide the system with faithful genome safeguarding. To explore how several additional molecular mechanisms can contribute in terms of providing the mitotic checkpoint with high fidelity, a mathematical modelling framework is constructed to simulate the spatially distinct production of anaphase inhibitors, their diffusion in the cytoplasm and inhibition of the anaphase-promoting machinery. The additional mechanisms capability to tightly inhibit anaphase promotion and rapidly release from metaphase arrest are central measures of model success, together with noise resistance and insensitivity to parameter perturbations. In conclusion, it is found that the mitotic checkpoint can be supported by a complex wait-anaphase signal, based on at least two parallel pathways, but other mechanisms can not be excluded. Finally, limitations of the approach are discussed and future work is suggested.

Table of Contents

1 Introduction

Chapter summary:

Avoiding harmful mutations during genome synthesis and segregation is significant in preventing cell proliferation related disease states, such as cancer. The mitotic checkpoint is the major safety mechanism in place to ensure faithful chromosome segregation in cell division. Despite detailed knowledge of the basic structure of the mitotic checkpoint, the full molecular understanding of how the mechanism is able to both provide strict metaphase arrest and rapid anaphase onset is still unsettled.

1.1 Fidelity is the key

1.1.1 Vast number, small chance

All somatic cells[1] are descendents of the same fertilized egg cell, through a single meiotic cell division, followed by a vast number of mitotic cell divisions. Every second, thousands of cells in the human body are replaced. The number of cells contained in a mammal the size of an adult human being is estimated to be in the order of 10^{14}. Clearly, the total number of cell divisions that has led to the fully grown individual is much higher than the number of cells that exist in the body at any time. The human genome can be represented by a more than 3 billion character long string, made up of the letters A, T, C and G, which denotes the sequence of the four different base pairs that comprise the DNA [1]. For every mitotic cell division, the entire genome in duplicated, with a remarkably small chance of error. No man made technology can compete at the level of speed and accuracy required by cells, especially not when considering that a cell is typically only a few picoliters in volume. To ensure that minimal error occur in every cell division, several safety mechanisms are in place. In particular, to safeguard the physical segregation of the chromosomes, all eukaryotes have inherited the same primary mechanism; the mitotic checkpoint. In essence, the function of the mitotic checkpoint is to govern the timing of critical events in mitosis in such manner that chromosome segregation can happen without compromising the genome content.

[1] Somatic cells can, loosely speaking, be defined as "the cells of the body", i.e., the cells contained in skin, bones, blood, and tissue.

1.1.2 Aneuploidy, cancer and mitosis

Aneuploidy is a cell state where the genome content deviates from the normal. An aneuploid cell has an incomplete or partially duplicated genome. The most commonly known human disease related to aneuploidy is Down's syndrome, which is characterized by a duplication of the whole or parts of chromosome 21 [1,2]. But also cancer is related to aneuploidy, although the connection is less direct. Cancer is a disease that is characterized by abnormal increase in cell number. The disease is caused by an unfortunate accumulation of gene mutations that alter the cellular regulatory systems that would normally maintain the processes of mitosis and apoptosis[2] in balance. Most cancers can be traced back to a single gene mutation that allows an individual cell to divide slightly faster then the neighboring cells in the tissue. The dangers of such pre-cancerous gene mutations are normally rendered harmless by intrinsic barriers that block the defected cells in continued proliferation. Unfortunately, these barriers are sporadically inactivated due to additional mutations, and the pre-cancerous cell is allowed to multiply. As much as 30 mutations can be necessary before a tumor is fully developed, as in the case of prostate cancer, that normally occurs in old age. The majority of cancers need only six to eight mutations to evolve, where the first and last mutation can take place from a few years to several decades apart [2]. Studying the control mechanisms that governs the genome integrity through the cell cycle, the mitotic checkpoint being a major piece of the puzzle, is thought to provide novel insight into the origin of several diseases, including many cancers.

[2] Programmed cell death.

1.2 The cell cycle and the mitotic checkpoint

1.2.1 The Cyclin clock

All eukaryotic cells have inherited the same basic cell cycle control system. From a cell is born in mitosis a variety of critical events take place, in a particular order, before the fully grown cell again divides. During every cell cycle the DNA is duplicated in synthesis, also called S-phase, and segregated in mitosis, called M-phase. Synthesis and mitosis are separated by two growth gaps, typically referred to as G_1- and G_2-phase. Historically, two main biological models are referenced when explaining the regulation of the progress of the cell cycle. The first model arises from the fact that all cells goes through the same phases, in the same order, with more or less the same timing. This observation is explained by the existence of an intrinsic clock that decides when it is time to move from one event to the next. The molecular mechanism that accounts for this clock-like behavior is the Cyclin dependent kinases and their activating binding partners, the Cyclin-family. The four variants, Cyclin A, B, D and E, are up- and down-regulated at distinct points in the cell cycle and, hence, display cyclical concentrations (Figure 1). The Cyclins act as trigger-proteins on the top of numerous signaling cascades, resulting in initiation and/or termination of cellular functions at appropriate times in the cell cycle [1,3]. In particular, formation of Cyclin B initiates mitosis and its degradation marks the mitotic exit. In such, Cyclin B is the master regulatory molecule that defines the mitotic state.

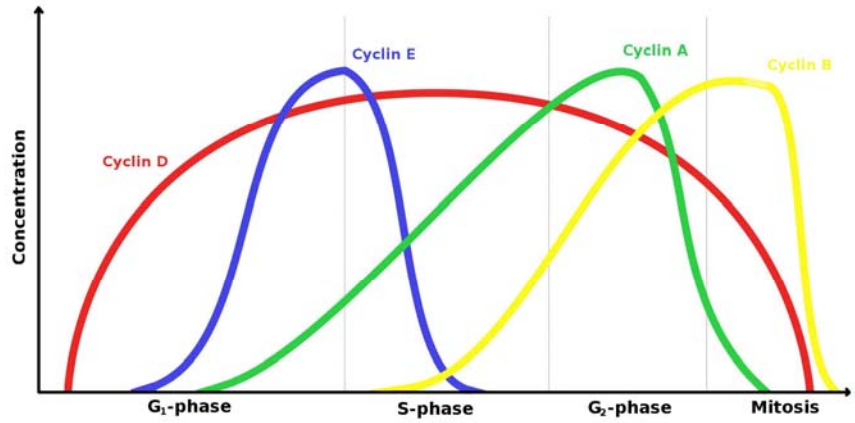

Figure 1: The clock-like behaviour of cell cycle progression is anchored in the up- and down-regulation of the Cyclin's. Most important for mitosis is Cyclin B, which marks mitotic entry and exit.

1.2.2 Checkpoints

In parallel to the cyclin-clock, an established model is that progression to the next phase in the cell cycle is controlled by specialized mechanisms that are activated by the completion of preceding events. This domino-effect is accounted for by the checkpoints; distinct points in the cell cycle where progression can be halted for variable time until crucial conditions are met (Figure 2). The checkpoints are often referred to as surveillance mechanisms that monitor and correct potentially dangerous behavior of the cell [1].

The first checkpoint is in G_1-phase, often referred to as the restriction point. The G_1-checkpoint monitors if the cell has grown sufficiently and if the environment is favorable for continuing into S-phase. If the cell is allowed to pass the restriction point, progression through the entire cell cycle is irreversible, unless the cell self-destructs in apoptosis. In G_2-phase the cell encounters the next checkpoint, where a test of the success of genome duplication and another assessment of the environmental conditions is performed. If errors are detected from synthesis, extensive machinery is started to repair the DNA-damage. If the checkpoint precautions are met, the cell continues into mitosis. Last in the cell cycle is the mitotic checkpoint, which ensures that the next generation cells faithfully receive one copy each of every chromosome [1].

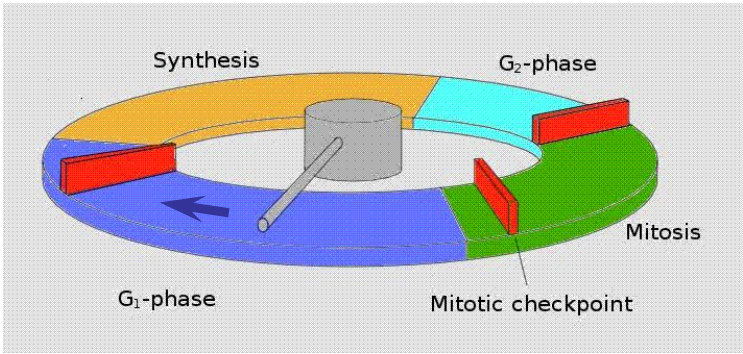

Figure 2: The mitotic checkpoint is one of three major checkpoints in the cell cycle. Checkpoints ensure errorless progression of the cell cycle by imposing delays at distinct points when crucial conditions are not met.

1.2.3 Mitosis and the mitotic checkpoint

Mitosis is a complicated and dramatic process, where the segregation of the chromosomes can be regarded as the climax of a long series of events. Typically, mitosis is divided into six sub-phases: prophase, prometaphase, metaphase, anaphase, telophase and cytokinesis, where the mitotic checkpoint regulates the transition from metaphase to anaphase (Figure 3). As the cells enter prophase, the genome is already duplicated and the two DNA-strands are loosely distributed in the nucleus. In prometaphase, the chromosomes are packed into a dense structure and the famous chromosomal X-shape appears. The centrosomes align at opposite sides of the nucleus and organize the mitotic spindle. The spindle assembles from the centrosomes by polymerization of the microtubules. Prior to metaphase, the nuclear envelope breaks down, allowing the microtubules to reach into the nucleus-region to capture the chromosomes at specific binding sites, called the kinetochores (Figure 4). Anaphase is initiated by the physical segregation of the mitotic spindle and the attached chromatids. The mitotic checkpoint controls the timing of this segregation by ensuring the stability of the spindle prior to complete attachments of all kinetochores[3]. Following the attachment of the last kinetochore, the mitotic checkpoint is inactivated and metaphase-anaphase transition is allowed. After anaphase come telophase and cytokinesis, where the two copies of the genomes is encapsulated in new cell nuclei, before the cell itself divides [1].

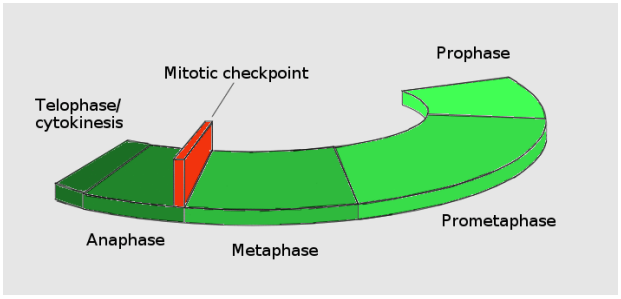

Figure 3: Mitosis is divided into six sub-phases: prophase, prometaphase, metaphase, anaphase, telophase and cytokinesis. The mitotic checkpoint regulates the metaphase-anaphase transition.

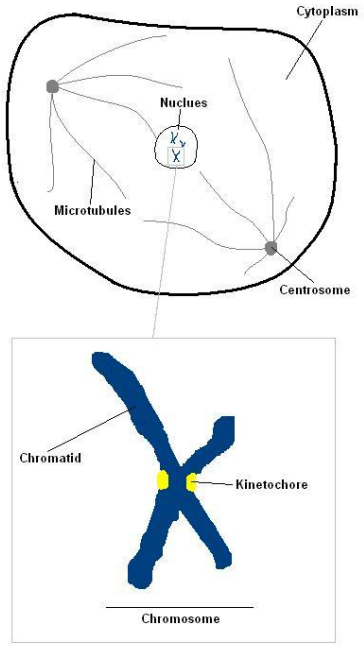

Figure 4: Schematic illustration of the key cellular components of the mitotic checkpoint. The microtubules grow out from the centrosomes and form the mitotic spindle. The spindle attach to the kinetochores, which are binding sites centrally located to each chromatid.

[3] The mitotic checkpoint is also referred to as the spindle assembly checkpoint.

1.2.4 Waiting for anaphase

The metaphase-anaphase transition is the most critical event of mitosis, since it marks the point of physical segregation of the genome. The basic mechanistic insight into how the appropriate initiation and termination of metaphase delay is controlled is well established [4]. The cell-cycle is halted until all chromosomes have obtained bipolar attachments to the mitotic spindle. When all attachments are made, the mitotic spindle pulls sister chromatids apart into two identical copies[4].

On the other hand, a detailed molecular understanding that can account for the mechanistic behavior is not fully developed. Early observations indicated that the timing of chromosome segregation is associated directly with the assembly of the mitotic spindle, through a negative feedback loop that is silenced when the spindle is fully developed. Further investigation displayed that the kinetochore binding sites where the spindle microtubules attach are the source of an emitted "wait-anaphase" protein signal and that this signal is silenced by kinetochore-microtubules attachment [5]. Unattached kinetochores are therefore reporters of an incomplete metaphase, something that is the direct cause of cell cycle arrest. Since the wait-anaphase signal is not silenced until all chromatids have obtained appropriate attachments, the mitotic checkpoint ensures bipolar segregation of the complete genome in anaphase (Figure 5).

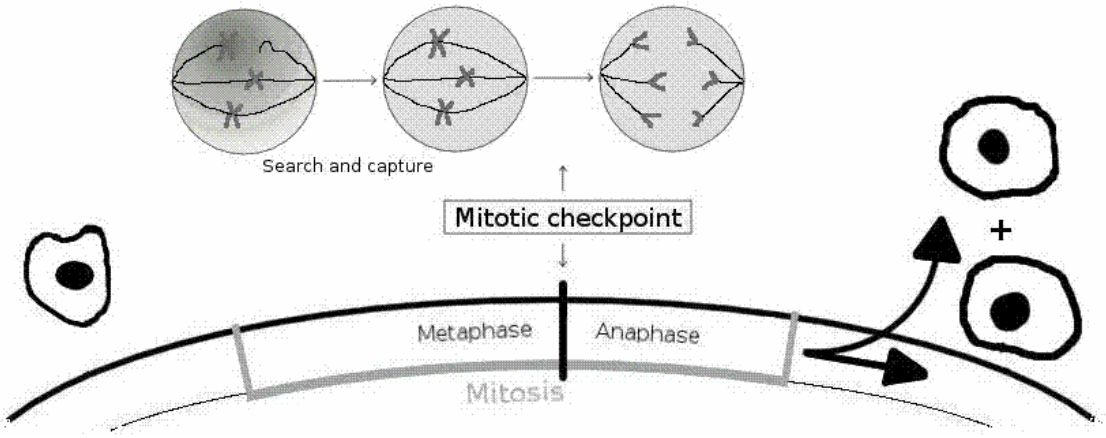

Figure 5: The mitotic checkpoint controls the transition from metaphase to anaphase. In essence, the mitotic checkpoint halts cell-cycle progression until all chromosomes are attached to the mitotic spindle. The spindle microtubules search the cytoplasm and capture kinetochores in a stochastic fashion. Kinetochores emit a diffusible protein signal when unattached that communicates throughout the cell that chromosome segregation is premature. In such, the cell is able to ensure that no chromosome is left behind in mitosis.

[4] The mitotic checkpoint also requires appropriate tension between the sister chromatids for segregation to be initiated. This mechanism controls that the chromatid-spindle attachment are truly bipolar and, therefore, cause a diametric pull on the chromosomes. Despite its central role in the mitotic checkpoint, the aspect of tension is omitted here, for simplicity.

1.2.5 Tight inhibition, rapid release

The search-and-capture time that elapse before all kinetochores have obtained bipolar spindle attachments average to approximately one hour, but is occasionally much longer [1,4]. Following the attachment of the last kinetochore, metaphase is exited by the physical segregation of the genome; an event that takes place within the order of minutes after the last attachment is made [5]. The observation that cells can wait for several hours in metaphase with a single kinetochore unattached, then rapidly progress into anaphase within minutes after the final attachment, impose two fundamental requirements on the mitotic checkpoint. First, the wait-anaphase signal must provide tight inhibition of the anaphase-promoting machinery, so that metaphase arrest can be stringently maintained for several hours. Second, the silencing of the wait-anaphase signal must result in the rapid removal of the inhibition, to allow release from metaphase arrest within the observed timeframe [4].

Tight inhibition and rapid release are basic mitotic checkpoint features. In current models, respecting both features simultaneously can result in a physical contradiction, which indicates that the underlying molecular machinery is not fully understood. Recent reports have suggested several molecular mechanisms that potentially can explain how the wait-anaphase signal is constructed so that both features are maintained. In the following, a mathematical modeling framework is developed to test these mechanisms capabilities of providing a functional mitotic checkpoint.

2 Biological models

Chapter summary:

Three main biological models are currently suggested in the literature, which all potentially can explain the apparent paradox of combining tight inhibition of the anaphase-promoting machinery with rapid release from metaphase arrest. In this chapter, these models are reviewed and expressed in terms of molecular interactions.

2.1 Core-circuitry

2.1.1 The Anaphase-Promoting Complex/Cyclosome and downstream

The Anaphase-Promoting Complex/Cyclosome (APC/C) is a large multi protein E3 ubiquitin ligase[1], responsible for initiating a biochemical pathway that results in dissolution of the link that keeps sister chromatids together. The ability of APC/C to trigger this pathway is regulated by its activating binding partner Cdc20. In essence, APC/C-Cdc20 initiates the first of three subsequent molecular events: *i)* degradation of Securin, *ii)* which cause activation of Separase, *iii)* that, in turn, degrades Cohesin. The latter is, as the name reveals, responsible for maintaining the coherency of the chromosomes. In a simplistic view, it can be assumed that the chromosomes are under mechanistic tension, due to a bipolar pull from the mitotic spindle, at the time Cohesin is degraded. When the Cohesin-link is removed, the chromosomes are segregated toward the spindle poles and further into the forming cells (Figure 6) [6]. In parallel to initiating chromosome segregation APC/C is responsible for degradation of Cyclin B and is, therefore, the regulator of general mitotic exit.

The molecular interactions that are directly involved in the inhibition and activation of the APC/C, hereafter denoted as the "core-circuitry", can be described in terms of a relatively small set of molecular interactions. Firstly, the APC/C (*a*) binds Cdc20 (*c*) and forms the

[1] APC/C being an E3 ubiquitin ligase means that it represents the third (and last) step in the ubiquitin-pathway. The details of this pathway fall outside the scope of this text, but loosely speaking it can be said that the ubiquitin-pathway marks specified protein with "the tag of death", which means that they will be destroyed.

active complex APC/C-Cdc20 (a^c) [6] in the cytoplasm

$$\text{Cyt:} \quad a + c \underset{\overline{\alpha}^c}{\overset{\alpha^c}{\rightleftarrows}} a^c .$$

The reaction is marked "Cyt:" to indicate that the spatial compartment where it takes place is the cytoplasm. The association rate α^c and dissociation rate $\overline{\alpha}^c$ of the APC/C-Cdc20 interaction will be handled in a later chapter when the biological modes are quantified, together with the reaction rates defined in the following.

Subsequent of its activation, APC/C degrades Securin (s), a process that can be described with the reaction

$$\text{Cyt:} \quad a^c + s \xrightarrow{\lambda} a^c + \varnothing .$$

The empty set sign $\varnothing$ indicates that Securin is degraded and exits the system. APC/C-Cdc20 is unaffected by the interaction. The reactions that are downstream of Securin degradation is not included directly in the core-circuitry, but seen as a direct consequence of the removal of Securin.

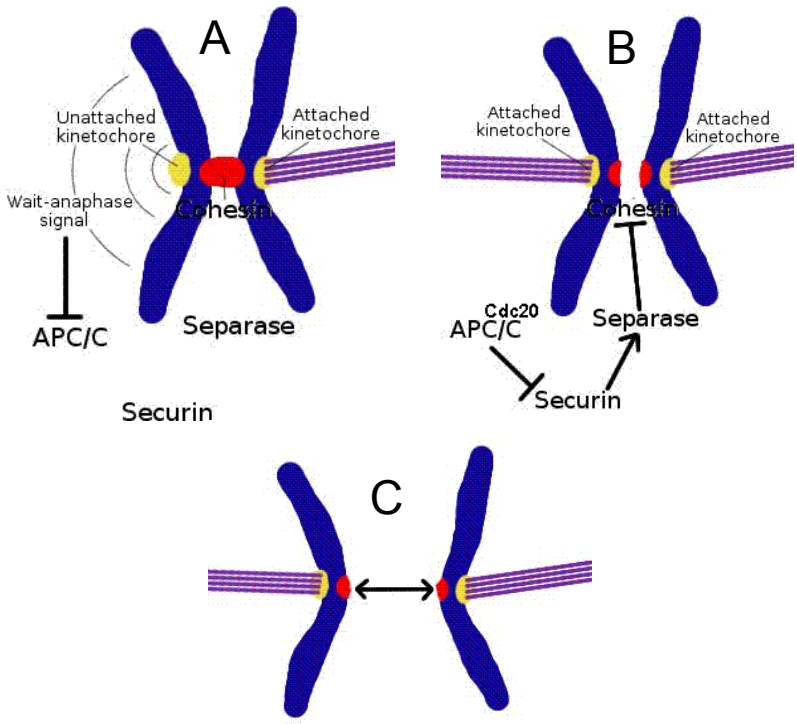

Figure 6: Unattached kinetochores emit a wait-anaphase signal that blocks the activity of the APC/C (A). The kinetochores are silenced by microtubules attachment (B). Following kinetochore silence, APC/C is activated by Cdc20, something that leads to degradation of Securin, subsequent activation of Separase and degradation of Cohesin (B). The latter is responsible for the coherency of the sister chromatids, consequently, its destruction allows the separation of the chromosomes due to a mechanistic pull from the mitotic spindle (C).

2.1.2 APC/C inhibition by the Mitotic Checkpoint Complex

The objective of the mitotic checkpoint is to strictly prevent exit from metaphase as long as one or more chromosomes are in lack of bipolar attachments to the mitotic spindle. The initial indication to what molecular mechanisms that are controlling mitotic arrest was obtained through two independent genetic screenings in Saccharomyces Cerevisiae (budding yeast) [7,8]. These screens identified various genes that caused mutated cells under a drug-induced absence of the mitotic spindle to consistently abrogate checkpoint arrest. The removal of the spindle should, obviously, provide a system with no kinetochore-microtubules attachments, since there are no microtubules. With no kinetochores attached, the wait-anaphase signal is at full strength and cells are expected to promptly arrest in metaphase. Down-regulation of genes that caused disobedience of such a fully operational checkpoint provided strong evidence that these genes are essential components of the wait-anaphase signal. Two gene families were revealed to play central roles. The first set of genes was the Mitotic Arrest Deficient-family (Mad1-3), later shown to be a key components of the kinetochore binding site that transmit the wait-anaphase signal, as well as a major part of the

signal itself. In addition, the Budding Uninhibited by Benzimidazole-family (Bub1-3) was given similar attention. The Mad1-3 and Bub1-3 genes are preserved in all eukaryotes (however, their names vary from species to species), where they are collectively involved in the mitotic checkpoint signaling pathway at nearly all levels [4,9].

Additional understanding of the mitotic checkpoint signaling mechanism was obtained through the observation that many of the Mad and Bub homologs in Xenopus Laevis (the African clawed frog) and human cells were enriched at the kinetochores in mitosis. Later, evidence was found that Mad2 associates with at least Cdc20 and BubR1[2] when located at the kinetochores, suggesting that a complex state of those components are formed. The formation of the Mad2-BubR1-Cdc20 complex, commonly denoted the Mitotic Checkpoint Complex (MCC), is established in the literature as an activated form of Mad2, since the MCC is a more potent binding partner to the APC/C than Mad2 alone. The MCC is also a more potent APC/C binding partner than Cdc20, and can therefore repress, or potentially completely block, APC/C activation [4,10].

The next major piece of the puzzle was obtained in an elegant experiment where the last kinetochore in lack of spindle attachment was destroyed by laser irradiation [5]. This intervention caused anaphase onset with timing that closely corresponded to the time that normally elapse from complete spindle assembly to anaphase onset in unaltered cells. This provided a strong indication that the wait-anaphase signal is emitted from the unattached kinetochores and that when kinetochores become attached to microtubules, this signal is silenced.

The APC/C-inhibition process consists of several steps that should be added to the core-circuitry. First, Cdc20 and BubR1 (b) forms a small complex (b^c) in the cytoplasm [11]

$$\text{Cyt:} \quad b + c \underset{\bar{\beta}^c}{\overset{\beta^c}{\rightleftarrows}} b^c .$$

Then, the BubR1-Cdc20-complex and Mad2 (m) binds to the unattached kinetochores, where formation of MCC (m^*) takes place at designated docking sites[3]

$$\text{Kin:} \quad m + b^c \xrightarrow{\mu} m^* .$$

The reaction is located to the kinetochores and is therefore marked “Kin:”.

[2] BubR1 is the human Mad3.
[3] Kinetochores are broadly assumed to be the main MCC-producers, despite the fact that direct evidence of this is lacking in the literature.

The parameter μ is the rate at which a single kinetochore produces the MCC. Silencing of the kinetochore due to spindle attachment is modeled by setting $\mu = 0$.

The MCC is assumed to have limited lifetime and dissociate spontaneously in the cytoplasmic event

$$\text{Cyt:} \quad m* \xrightarrow{\bar{\mu}} m + b + c\,.$$

The inhibition process is completed when MCC binds APC/C to form the inhibited APC/C-MCC-complex ($a*$) in the cytoplasmic reaction

$$\text{Cyt:} \quad a + m* \underset{\bar{\alpha}*}{\overset{\alpha*}{\rightleftarrows}} a*.$$

2.1.3 p31 catalyze the disassembly of APC/C-MCC

Recent discoveries have pointed out the small protein $p31_{comet}$ (hereafter just p31) to be an additional key player in the mitotic checkpoint signaling network. Initially it was found that over-expression of p31 in vivo caused precocious anaphase onset and that a knock-down of the protein caused cells to lose the ability to proceed into anaphase after complete kinetochore attachment, or at least slow the process down significantly [12]. On the molecular level, p31 is known to attack the MCC-component of the APC/C-MCC complex [13]. In vitro, p31 merely binds to the APC/C-MCC, however, it is hypothesized that this interaction result in the complete disassembly of the inhibited complex in vivo [14,15].

In such, the interference of p31 with the core-circuitry can be said to catalyze the degradation of the APC/C inhibition. The catalytic effect of p31 (p) is thought to take place in a two-step process involving an unstable intermediate complex APC/C-MCC-p31 (a^p),

$$\text{Cyt:} \quad a* + p \underset{\bar{\alpha}^p}{\overset{\alpha^p}{\rightleftarrows}} a^p \xrightarrow{\bar{\alpha}} a + m + b + c + p\,.$$

In addition, the MCC-p31-complex (m^p), which is a sub-complex of APC/C-MCC-p31, can be formed without the presence of APC/C. However, p31 does not catalyze the disassembly of the MCC when unbound to the APC/C [14],

$$\text{Cyt:} \quad m^* + p \underset{\bar{\alpha}^p}{\overset{\alpha^p}{\rightleftarrows}} m^p .$$

The reaction rates involved in the MCC-p31 interactions can be assumed to be identical to those of the APC/C-MCC-p31 interaction, regardless of the presence of APC/C.

Finally, the MCC-p31 complex is assumed to bind APC/C directly and form the APC/C-MCC-p31 complex

$$\text{Cyt:} \quad a + m^p \underset{\bar{\alpha}^*}{\overset{\alpha^*}{\rightleftarrows}} a^p \left(\xrightarrow{\bar{\alpha}} a + m + b + c + p \right),$$

with the same reaction rates involved as when APC/C binds MCC without the presence of p31.

2.1.4 The insufficiency of the core-circuitry

In a qualitative setting, the core circuitry is in principle sufficient to explain how mitotic checkpoint signaling can work. That is, the APC/C is inhibited from Cdc20 activation by formation of a more potent binding partner, the MCC, at unattached kinetochores. When kinetochore attachment is complete, MCC production is stopped and the APC/C-MCC-complex is degraded by p31, followed by APC/C activation.

In a quantitative setting, however, the core-circuitry model becomes incapable of providing sufficient inhibition simultaneously as release is allowed within the observed timeframe, which can be illustrated by a rough estimation of the balance between formation and degradation of core-circuitry components [16]. The single kinetochore MCC production rate, which is measured to be approximately 100 molecules per second [17,18], must at least balance the cytoplasmic degradation of APC/C-MCC to support proper inhibition. Assuming that the concentration of APC/C in the cytoplasm is *100nM* and that the cytoplasmic volume is *6pL*, a estimate of the number of APC/C-molecules can be calculated:

$$N_{APC/C} = 100nM \cdot 6\,pL = 100\frac{10^{-9} \cdot 6.02 \cdot 10^{23}}{L} 6 \cdot 10^{-12} L \approx 400000 .$$

For the mitotic checkpoint to be able to tightly inhibit the larger fraction of APC/C molecules prior to complete kinetochore attachment, the degradation rate of APC/C-MCC can, therefore, be at most

$$\bar{\alpha}^{*}_{max} = \frac{100/s}{400000} = 0.00025/s\,.$$

This rate corresponds to a degradation time of 46 minutes, which is longer than what is observed in cells [5]. The conclusion is therefore that if a single kinetochore can maintain tight inhibition, rapid release is excluded, based on the molecular mechanisms defined in the core-circuitry alone.

Alternatively, the dissociation rate of the APC/C-MCC that is needed for rapid release to be allowed can be considered. The lag from complete kinetochore attachment to anaphase initiation is regulated by the time consumed by APC/C-MCC degradation and APC/C-Cdc20 activation and the downstream pathway. APC/C-Cdc20 complex formation is, as explained in more detail later, assumed to be diffusion limited, which is the fastest reaction possible in a reaction-diffusion system [19]. The total time that elapse from the final kinetochore becomes attached to anaphase initiation is on average 23 minutes [5]. It is clear that complete degradation of APC/C-MCC can at the most consume this amount of time. However, since the downstream pathway of APC/C-Cdc20 must be allowed time for execution, the degradation APC/C-MCC can be assumed to occur within 10 minutes [16], as a first approximation. Assuming that the degradation process of APC/C-MCC can be approximated by a single exponential decay, the dissociation rate required to allow rapid release can be estimated by

$$t_{1/2} = \frac{\ln 2}{10 \cdot 60} s^{-1} = 0.0012 s^{-1}\,.$$

The APC/C-MCC dissociation rate of $0.0012s^{-1}$ is close to the dissociation rate of the APC/C-Cdc20-complex that is observed in the system [20]. On the other hand, there is no reason to believe that the association rate of MCC binding to ACP/C is any different than that of Cdc20 binding to APC/C, since the MCC binds through its Cdc20 sub-molecule [14]. Combining the consistency in both association and dissociate rates indicates that the affinity of APC/C to MCC and Cdc20 is similar. However, this is contradictory to the fundamental assumption that the MCC is a more potent binding partner to the APC/C than Cdc20, since the affinity of the APC/C-MCC interaction must exceeds that of the APC/C-Cdc20 interaction significantly. Hence, allowing rapid release alters the ability of the MCC to tightly inhibit APC/C.

Several molecular mechanisms have been proposed to resolve the question of how the wait-

anaphase signal can support both the appropriate inhibition strength and release time. At the current, the suggested mechanisms can be summarized in three major biological models, *i)* cytoplasmic MCC amplification, *ii)* cytoplasmic MCC assembly and *iii)* regulation of APC/C-MCC lifetime by a complex wait-anaphase signal.

2.2 Cytoplasmic MCC amplification

2.2.1 Intra-cellular signal amplification

The problem of how a signal emitted from a small structure like the kinetochore can efficiently communicate its message to the entire cell is a general question in cell biology. A well studied example is the MAPK-signaling cascades, which in response to specific external conditions can trigger a variety of intracellular pathways, including cellular growth and apoptosis [1]. The initiating step of the MAPK-pathways is that a receptor in the cell membrane becomes reactive to an external signal. The intra-cellular domain of the receptor, a structure comparable in size to the kinetochore, emits a protein signal. Before reaching its destination, the protein species of this signal goes through a series of phorphorylation steps that "energize", or amplify, the signal. In a similar fashion, it is an attractive possibility that the wait-anaphase signal undergoes a post-kinetochore amplifying modification. Such a mechanism could potentially solve the problem of combining tight inhibition and rapid release, since the APC/C-MCC degradation rate no longer needs to be balanced directly by the single kinetochore production capacity.

2.2.2 MCC as a scaffold for MCC-formation

In addition to being a component of the cytoplasmic wait-anaphase signal, Mad2 appears in an insoluble state, bound to Mad1 at the kinetochores. The kinetochore-bound Mad1-Mad2 complex is hypothesized to serve as a template for the unification of Mad2, BubR1 and Cdc20 to become MCC. In the MCC-formation, Mad2 is in a closed state, called C-Mad2, while unbound Mad2 is in an open state, namely O-Mad2. The transition from O-Mad2 to C-Mad2 was originally thought to take place exclusively at the Mad1-Mad2 template at the kinetochore. But, in a recent report [21] it was suggested that the MCC can mimic this capability away from the unattached kinetochores. This mechanism can potentially account for a post-kinetochore amplification step where MCC binds O-Mad2 and BubR1-Cdc20 in the cytoplasm to produce additional MCC. A strongly simplified model of this mechanism can be constructed by defining a reaction where pure Mad2 and the BubR1-Cdc20-complex are joined to form new MCC and the already present MCC contributes as a passive component

$$\text{Cyt:} \quad m^* + m + b^c \xrightarrow{\mu_{amp}} 2m^*.$$

The parameter μ_{amp} determines the strength of the amplification in bulk.

2.3 Cytoplasmic MCC assembly

2.3.1 Kinetochore independent MCC formation in yeast

Despite the strong evidence that kinetochores are the spatial location from where the wait-anaphase signal is emitted, the common conception that MCC is assembled at kinetochores is controversial. The requirements of MCC assembly at kinetochore were tested in an experiment with mutated yeast cells where the kinetochore structures were destabilized and unable to perform their hypothesized function as MCC producers [22]. The result displayed that cells with non-functional kinetochores produced similar amounts of MCC as the unaltered cells, indicating that the MCC is assembled away from the kinetochores, at least in the yeast system.

2.3.2 Unattached kinetochores activate MCC

The cytoplasmic assembly model suggests that Mad2 and BubR1-Cdc20 form an inactive MCC (m') in the cytoplasm

$$\text{Cyt:} \quad m + b^c \underset{\bar{\beta}^c}{\overset{\beta^c}{\rightleftarrows}} m' .$$

Mad2 is thought to bind the Cdc20 sub-molecule of the BubR1-Cdc20 complex in a similar fashion as BubR1 [11], so the rates of the interaction coincide with those of the BubR1-Cdc20 complex formation.

The inactive MCC visits the unattached kinetochores subsequent of the cytoplasmic formation, where it is activated,

$$\text{Kin:} \quad m' \xrightarrow{\mu} m^* .$$

In this model, only one molecular species must be present at the kinetochore for active MCC to be formed, as opposed to the two substrates that must be present for MCC assembly. Activation can therefore potentially represent an easier task for the kinetochore, as opposed to full MCC assembly, since the production rate is now limited by diffusion of one species only.

2.4 Regulation of APC/C-MCC lifetime by a complex wait-anaphase signal

2.4.1 Variable APC/C-MCC lifetime

The rate at which MCC turns over at a single kinetochore is measured to be approximately 100 molecules per second [17,18]. As already indicated, this production rate does not balance the cytoplasmic APC/C-MCC dissociation rate needed to allow rapid release. However, it is a formal possibility that the dissociation rate of APC/C-MCC is modulated in mitosis, for example by a pathway parallel to the MCC production, such that APC/C-MCC degradation is slower when the wait-anaphase signal is on than when it is off.

Regulation of the catalytic effect of p31 could be the target for an APC/C-MCC dissociation rate modulation pathway [23]. A high concentration of active p31 causes the APC/C-MCC complex to degrade rapidly, while a low p31 concentration results in slow degradation. A complex wait-anaphase signal, that is both promoting the MCC-inhibitor and inhibiting the p31-promotion of the APC/C, could potentially account for the ability to tightly inhibit and rapidly release.

2.4.2 Unattached kinetochores as p31 regulators

Recent findings show that p31 is enriched at kinetochores in mitosis and that it turns over with fast kinetics (data shown in Ch. 3.2.3, Figure 9). Earlier assays have revealed that p31 can be phosphorylated[4] by proteins known to be present at kinetochores [24], supporting the hypothesis that the kinetochore turnover might represent a modification that inactivates p31 (p^*)

$$\text{Kin:} \quad p \xrightarrow{\sigma} p^* .$$

When kinetochores are attached to the spindle, the inactivation of p31 is assumed to be ceased. This is modeled by setting $\sigma = 0$. The inactivated p31 is thought to reactivate in the cytoplasm

$$\text{Cyt:} \quad p^* \xrightarrow{\bar{\sigma}} p .$$

[4] Phosphorylation can both mean activation and inactivation, depending on the context. Here, phosphorylation means inactivation.

2.5 Buffering of excess Cdc20

2.5.1 Cdc20 play a dual role

Cdc20 is both the activator of APC/C and a component of its inhibitor (the MCC). Any number of Cdc20-molecules in excess of the number of Mad2- and BubR1-molecules cannot be bound up in MCC-molecules and will, therefore, compromise the ability to inhibit APC/C. On the other hand, if there is a lack of Cdc20 molecules in comparison to the other signal components, inhibition can be strong, but the Cdc20 pool might not be large enough to activate APC/C sufficiently.

Due to this dual role, it is likely that the system performs poorly both with too low and too high concentration levels of Cdc20. An important feature of the mitotic checkpoint is that the system is robust to variation in parameters, particularly concentration levels. For a parameters that is highly sensitive to variations, a buffering mechanism might be necessary.

2.5.2 Kinetochore buffering mechanism

Cdc20 is shown to turn over at kinetochores, in parallel to Mad2 and BubR1. The turnover of Cdc20 is a central observation that led to the understanding of how the MCC is formed. However, in the same experiment it was demonstrated that Cdc20 turnover at kinetochores is biphasic [17,18]. The slow rate corresponds to the rate of the Mad2 and BubR1 turnover and is concluded to represent the formation of MCC. The faster rate is, however, independent of other molecular species that dynamically associate at kinetochores. In addition, the faster turnover is unaltered by kinetochore attachment. Like p31, Cdc20 is known to be phosphorylated by kinetochore-present proteins [26]. This has led to the hypothesis that the fast Cdc20 turnover represents an inactivation mechanism,

$$\text{Kin:} \quad c \xrightarrow{\gamma} c^* .$$

The inactive Cdc20 (c^*) is assumed to reactivate in the cytoplasm

$$\text{Cyt:} \quad c^* \xrightarrow{\bar{\gamma}} c .$$

The function of the Cdc20 turnover is thought to be buffering of Cdc20 that cannot be captured in the MCC-pathway.

3 Materials and methods

Chapter summary:

Reaction-diffusion equations are suitable for modeling cytoplasmic signaling networks. By introducing a set of specified Robin boundary conditions, a mathematical framework for simulation of the kinetochore-emitted wait-anaphase signal is obtained. To assess the parameters that appear in the mathematical models a number of biological assays must be combined. The resulting partial differential equations can be simulated numerically in MATLAB. To reduce processing time, large scale simulations are performed on a computing cluster.

3.1 Reaction-diffusion equations

3.1.1 Derivation of the reaction-diffusion equation

The reaction-diffusion equation is a type of second order parabolic partial differential equation that frequently appears in a broad range of applications. One usage is describing the concentration of molecules that are diffusing and reacting in solution, others are to describe heat transfer from a source in a homogenous medium, price stock options that are assumed to fluctuate by Brownian motion and, at specific time scales, describe electromagnetic properties in a material with constants electrical conductivity [27].

In the context of modeling intra-cellular signaling networks, the reaction-diffusion equation can be derived by assuming mass conservation of specific proteins within an arbitrary test volume M in the cytoplasm. The temporal rate of change in mass must be balanced by the mass flux over the test volume boundary due to diffusion and a sink/source term in the interior due to reactions. Mathematically, the concentration of a molecular species is governed by the mass conservation law

$$\frac{d}{dt}\int_M \rho \, dV + \oint_{\partial M} \vec{\phi} \cdot \vec{n} \, dS = \int_M q \, dV \,, \tag{1}$$

where $\rho = \rho(\vec{r},t)$ is the local concentration, $\vec{\phi} = \vec{\phi}(\vec{r},t)$ is the flux-density and $q = q(\vec{r},t)$ is a function that describes the local change in concentration due to chemical reactions. It is assumed that there is no macroscopic movement of the cytosoluble fluids in the model, so $\vec{\phi}$ is given by the movement of particles due to diffusion only. Further, it is assumed that the cytoplasm is a homogenous solution and that the protein molecules can diffuse freely in it.

For functions that are at least C^1-smooth, which can safely be assumed to be the case here, the order of integration and derivation in (1) can be interchanged,

$$\int_M \frac{\partial \rho}{\partial t}\, dV + \oint_{\partial M} \vec{\phi} \cdot \vec{n}\, dS = \int_M q\, dV\,. \tag{2}$$

Since the local protein flux is only due to diffusion, the flux term $\vec{\phi}$ is simply given by Fick's law

$$\phi \cdot \vec{n} = -D\, \nabla\rho \cdot \vec{n}\,, \tag{3}$$

where D is the diffusion constant.

Substitution of (3) into (2) results in

$$\int_M \frac{\partial \rho}{\partial t}\, dV - \oint_{\partial M} D \nabla\rho \cdot \vec{n}\, dS = \int_M q\, dV\,. \tag{4}$$

Next, applying the divergence theorem to the diffusion term in (4) provides an equation where all terms are integrals of the interior of *M*,

$$\int_M \frac{\partial \rho}{\partial t}\, dV - \int_M \nabla \cdot (D\, \nabla\rho)\, dS = \int_M q\, dV\,. \tag{5}$$

Since it is assumed that diffusion is constant throughout the cytoplasm, (5) can be written as

$$\int_M \frac{\partial \rho}{\partial t}\, dV - \int_M D\, \Delta\rho\, dS = \int_M q\, dV\,, \tag{6}$$

where $\Delta = \nabla^2$ is the Laplace-operator.

Finally, by assuming that (6) holds for every test volume (including a very small one) the integration signs can be removed,

$$\frac{\partial \rho}{\partial t} = D\Delta\rho + q\,, \tag{7}$$

which yields the general form of the reaction-diffusion equation.

The cytoplasmic interactions, incorporated in the reaction-diffusion equation by the *q*-term in (7), are assumed to follow mass-action kinetics [28]. The rate of change in protein concentration due to forward type reactions,

$$\text{Cyt:} \quad s_1 + s_2 \xrightarrow{\eta} p\,, \tag{8}$$

are given by the empirical formula:

$$-\frac{ds_1}{dt} = -\frac{ds_2}{dt} = \frac{dp}{dt} = \eta s_1 s_2\,.$$

The constant η is denoted the association rate. The reverse reaction,

$$\text{Cyt:} \quad p \xrightarrow{\overline{\eta}} s_1 + s_2\,, \tag{9}$$

is independent of the forward reaction and cause a change in protein concentration given by:

$$\frac{ds_1}{dt} = \frac{ds_2}{dt} = -\frac{dp}{dt} = \overline{\eta}\, p\,.$$

The constant $\overline{\eta}$ is denoted the dissociation rate.

Both the forward and reverse reactions take place in a solution where all particles are freely diffusible. The concentrations s_1, s_2 and p will then be governed by the following set of reaction-diffusion equations:

$$\frac{\partial s_1}{\partial t} = D_{s_1}\Delta_r s_1 - \eta s_1 s_2 + \overline{\eta} p\,,$$
$$\frac{\partial s_2}{\partial t} = D_{s_2}\Delta_r s_2 - \eta s_1 s_2 + \overline{\eta} p\,,$$
$$\frac{\partial p}{\partial t} = D_p \Delta_r p + \eta s_1 s_2 - \overline{\eta} p\,.$$

The kinetochore-bound reactions are introduced in the reaction-diffusion system through special boundary conditions. The main idea is that a kinetochore-bound reaction where substrates s_1 and s_2 form complex p at rate κ,

$$\text{Kin:} \qquad s_1 + s_2 \xrightarrow{\kappa} p\,, \tag{10}$$

produce a set of fluxes over the kinetochore-cytoplasm boundary. The kinetochore fluxes are balanced according to (10) and quantified by Fick's law,

$$-D_{s_1}\nabla s_1 \cdot \vec{n} = -D_{s_2}\nabla s_2 \cdot \vec{n} = D_p \nabla p \cdot \vec{n} = J_\kappa\,,$$

where $\vec{n}$ is the unit normal to the kinetochore-cytoplasm boundary.

Because the kinetochore flux is dependent on the attachment state of the kinetochore (a function of time) and the presence of substrate (a function of concentration), J_κ can be decomposed into

$$J_\kappa = J_\kappa(\vec{u},t) = j_\kappa \cdot \ell_C \cdot \ell_t\,,$$

where j_κ is the flux density corresponding to maximal kinetochore turnover and $\ell_C, \ell_t \in [0,1]$ are functions responsible for silencing the kinetochores according to microtubules attachment and lack of substrate, respectively. The regulatory function ℓ_t can simply be set to one before attachment of the kinetochore and zero after, with a short smoothed transition, primarily added to ease the numerical scheme used to solve the equations. The function ℓ_C is set to one if there are sufficient amounts of both substrates available for the kinetochore turnover, but approach zero as the substrate concentration at the kinetochore disappears. A suitable choice for ℓ_C is therefore

$$\ell_C = 1 - e^{-s_1 s_2}\,.$$

To obtain a more general notation that can be useful when modeling the mitotic checkpoint, it is assumed that the biological models defines N molecular species with concentration functions contained in vector $\vec{u}$,

$$\vec{u} = \vec{u}(\vec{r},t) = [u_1(\vec{r},t), \ldots, u_N(\vec{r},t)].$$

The corresponding vector reaction-diffusion equation can then be written

$$\frac{\partial \vec{u}}{\partial t} = D\Delta\vec{u} + \vec{R}(\vec{u}), \tag{11}$$

where D is a diagonal matrix of diffusion constants

$$D = \begin{bmatrix} D_1 & 0 & \cdots & 0 \\ 0 & D_2 & \cdots & 0 \\ \vdots & \vdots & \ddots & \vdots \\ 0 & 0 & \cdots & D_N \end{bmatrix}$$

and the function $\vec{R}$ describes the mass-action kinetics of the cytoplasmic reactions.

A quantitative framework for simulating the biological models presented in Ch.2 will be provided by solving the equations (11) over

$$\vec{r} \in S \subset \Re^3 \quad \text{and} \quad t \in [t_0, t_1]$$

with initial conditions

$$\vec{u}^0 = \vec{u}(\vec{r},0) = [u_1(\vec{r},0), \ldots, u_N(\vec{r},0)],$$

and boundary conditions on the first derivative

$$-D\frac{\partial \vec{u}}{\partial \vec{n}} = \vec{J}(\vec{u},t),$$

where $\vec{n}$ is unit normal to the boundary of S and $\frac{\partial \vec{u}}{\partial \vec{n}} = [\nabla u_1 \cdot \vec{n}, \ldots, \nabla u_N \cdot \vec{n}]$

3.1.2 Symmetry in solutions

In Ch. 3.1.1, the reaction-diffusion equation is derived in three spatial dimensions. Both the reaction and diffusion part of the system is approximated to be radial symmetric. As explained in Ch. 4., the geometry of the mathematical modeling framework is spherical. In such, spherical symmetry will be inherited by all solutions $u_i(\vec{r},t)$. Therefore, choosing to represent the reaction-diffusion equations in spherical coordinates will reduce the number of spatial dimensions in the mathematical formulation from three to one.

For a spherically symmetric system represented in spherical coordinates, the Laplace operator reduces to

$$\Delta_r = \frac{1}{r^2}\frac{\partial}{\partial r} r^2 \frac{\partial}{\partial r}.$$

Only the diffusion term in the reaction-diffusion equation is dependent on the spatial coordinate, so the spherically symmetric variant of (11) is found simply by writing the Laplace-operator in radial form. The reaction-diffusion problem is then reduced to solving

$$\frac{\partial \vec{u}}{\partial t} = D\Delta_r \vec{u} + \vec{R}(\vec{u}), \tag{12}$$

for

$$r \in [R_K, R_C] \text{ and } t \in [t_0, t_1] \tag{13}$$

with initial conditions

$$\vec{u}^0 = \vec{u}(r,0) = [u_1(r,0), \ldots, u_N(r,0)], \tag{14}$$

and boundary conditions

$$-D\frac{\partial \vec{u}}{\partial \vec{n}} = \vec{J}(\vec{u},t), \tag{15}$$

where $\vec{n}$ is unit normal for $r \in R_K, R_C$.

3.1.3 Existence and uniqueness of the intial-value problem

As a starting point for investigating the existence and uniqueness of the initial-boundary problem (12)-(15) a simpler test problem is considered, namely the scaled three-component reaction-diffusion problem describing the cytoplasmic reactions (8)-(9), without specified boundary conditions:

$$\frac{\partial \vec{u}}{\partial t} - \Delta \vec{u} = \vec{R}\,, \tag{16}$$

where

$$\vec{u} = [u_1, u_2, u_3] \tag{17}$$

and

$$\vec{R}(\vec{u}) = \begin{bmatrix} -u_1 u_2 + u_3 \\ -u_1 u_2 + u_3 \\ u_1 u_2 - u_3 \end{bmatrix}, \tag{18}$$

solved over $r \in [R_K, R_C]$ and $t \in [t_0, t_1]$ with initial conditions

$$\vec{u}(r,0) = \vec{u}_0 \qquad . \tag{19}$$

The details of how the reaction-diffusion system with physical coefficients (12)-(14) can be scaled into (16)-(19) are not included here, but the procedure is straight forward (see e.g. Ch 5.1.1). A brief discussion of the generalization of the following results to apply for any N-dimensional system is given in [29].

The operator that appear on the left side in (16),

$$\frac{\partial}{\partial t} - \Delta\,,$$

is, loosely speaking, a more stable operator than the time derivative by itself. As indicated more formally below, it is reasonable to assume that if the reaction-term does not cause spurious results in the reaction problem

$$\frac{d\vec{u}^R}{dt} = \vec{R}\,, \tag{20}$$

the same reaction-term will not cause spurious results in the corresponding reaction-diffusion problem either. The focus is, therefore, temporarily shifted to investigate if the dynamical system (20) has bounded solutions.

A set $\Omega \subset \Re^3$ is invariant to (20) if

$$\vec{u}^R(t) \in \Omega \text{ for all } t \geq 0\,,$$

when $\vec{u}_0^R = \vec{u}^R(0) \in \Omega$. Sufficient conditions to ensure that Ω is invariant to the reaction equation (20) is that

$$\vec{n} \cdot \vec{R}(\vec{u}^R) \leq 0 \text{ for } \vec{u}^R \in \partial\Omega\,, \tag{21}$$

where $\vec{n}$ is the unit normal pointing out of the region Ω. If (21) can be showed to be true, the existence of a bounded solution to (20) is guaranteed.

The first octant

$$u_1^R, u_2^R, u_3^R \geq 0 \tag{22}$$

can immediately be concluded to be invariant, since

$$\vec{n} \cdot \vec{R}(\vec{u}^R) = \begin{cases} -u_3^R \\ -u_3^R \\ -u_1^R u_2^R \end{cases} \leq 0$$

for $u_1^R = 0$, $u_2^R = 0$ and $u_3^R = 0$, respectively. Further, the functions

$$g_1 = u_1^R + u_3^R \text{ and } g_2 = u_2^R + u_3^R$$

are invariant quantities, since

$$\vec{R}(\vec{u}^R) \cdot \nabla g_1 = \vec{R}(\vec{u}^R) \cdot \nabla g_2 = -u_1^R u_2^R + u_3^R + u_1^R u_2^R - u_3^R = 0\,,$$

which simply means that g_1 and g_2 are constant (something that is also clear from the chemical relation (8) and (9)). The sum of invariant quantities,

$$g_1 + g_2 = u_1^R + u_2^R + 2u_3^R ,$$

is itself an invariant quantity. A region that can be tested for invariance is suggested by imposing the requirement

$$g_1 + g_2 = u_1^R + u_2^R + 2u_3^R \le K . \tag{23}$$

The subset defined by (22) and (23) defines a tetrahedron (in general a simplex),

$$\Omega = \left\{ u_1^R, u_2^R, u_3^R \in \Re \mid u_1^R \ge 0, u_2^R \ge 0, u_3^R \ge 0, u_1^R + u_2^R + 2u_3^R \le K \right\},$$

which is a convex subset of $\Re^3$.

Ω is invariant to the reaction term (18) since

$$\vec{n} \cdot \vec{R}(\vec{u}^R) = \frac{1}{\sqrt{6}}[1,1,2] \begin{bmatrix} -u_1^R u_2^R + u_3^R \\ -u_1^R u_2^R + u_3^R \\ u_1^R u_2^R - u_3^R \end{bmatrix} = 0 ,$$

where $\vec{n} = \frac{1}{\sqrt{6}}[1,1,2]$ is the normal vector of the plane

$$u_1^R + u_2^R + 2u_3^R = K .$$

The condition (21) is fulfilled and the existence of a bounded solution to the reaction equation (20) is guaranteed.

Adding diffusion back into the equation is claimed above to not cause any problems to the existence of a solution; however, a formal argument was not given. Now, let H_t be a solution operator

$$\vec{y}(\vec{r},t) = H_t \vec{y}_0(\vec{r})$$

that produces a solution $\vec{y}(\vec{r},t)$ to the partial differential equation

$$\frac{\partial \vec{y}}{\partial t} = \tilde{H}\vec{y} = \left(\tilde{H}^1 + \tilde{H}^2\right)\vec{y},$$

over space-time domain $S \times [0,T]$ and with initial conditions $\vec{y}_0$. According to Trotters formula can H_t be expressed as

$$H_t = \lim_{n \to \infty} \left[H^1_{t/n} \cdot H^2_{t/n}\right]^n,$$

where H^1_t and H^2_t are the solution operators to the differential equations

$$\frac{\partial \vec{y}}{\partial t} = \tilde{H}^1 \vec{y} \quad \text{and} \quad \frac{\partial \vec{y}}{\partial t} = \tilde{H}^2 \vec{y},$$

with initial conditions $\vec{y}_0$, over $S \times [0,T]$, respectively [30].

In words, Trotters formula states that applying the diffusion operator and the reaction operator in an alternating fashion, using the end value to one solution as initial conditions to the other, is equivalent to applying the full reaction-diffusion operator, as the time increments approach zero. Therefore, the invariance of Ω can be investigated with respect to the reaction and diffusion terms separately[1]. Since Ω is already established as invariant to the reaction equation, what must be shown to guarantee the existence of solution to the reaction-diffusion system is that Ω is also invariant to the diffusion equation.

Assume that the components of $\vec{u}^D$ all fulfill the scalar diffusion equation

$$\frac{\partial u_i^D}{\partial t} = \Delta u_i^D,$$

independently of each other. It is easy to see that any linear combination of the components of $\vec{u}$

$$h(\vec{u}^D) = \vec{b} \cdot \vec{u}^D$$

also fulfill the diffusion equation, since

[1] Strictly speaking, the convergence of the limit in Trotters formula should be investigated for every operator, but this is generally not a problem for reaction or diffusion operators.

$$\frac{\partial h(\vec{u}^D)}{\partial t} = b_1 \frac{\partial u_1^D}{\partial t} + \cdots + b_N \frac{\partial u_N^D}{\partial t} = b_1 \Delta u_1^D + \cdots + b_N \Delta u_N^D = \Delta h(\vec{u}^D). \qquad (24)$$

The solutions of (24) follows a maximum principle [29], formulated as: Let $S \subset \Re^N$ be an open and limited subset with closure $\overline{S}$, and let $T > 0$. If a function h is continuous on $\overline{S} \times [0,T]$ and is governed by the diffusion equation in $S \times (0,T)$, then h will reach its maximum value on the parabolic boundary:

$$\overline{S} \times \{0\} \cup \partial \overline{S} \times [0,T].$$

It follows from the maximum principle that if h reaches its maximum on $S \times (0,T)$, then h is constant.

A consequence of the maximum principle is that an initial condition $\vec{u}_0^D$ and vector $-\vec{b}$ defines a half-plane which the solution $\vec{u}^D$ is bounded in. The maximum principle holds for every u_0^D and $\vec{b}$. Since every convex subset of $\Re^N$ can be bounded by a set of half-planes, every convex subset is invariant to the diffusion equation (Figure 7).

For spherically symmetric functions in $\Re^3$ this means that if the initial conditions u_0^D has a maximum in (R_K, R_C), this will be the maximum for the entire solution. In such, the claim that diffusion smoothens the solutions out is appropriate.

Diffusion can therefore not move $\vec{u}^D$ out of Ω. Hence, Ω is invariant to the diffusion equation and therefore to the reaction-diffusion equation.

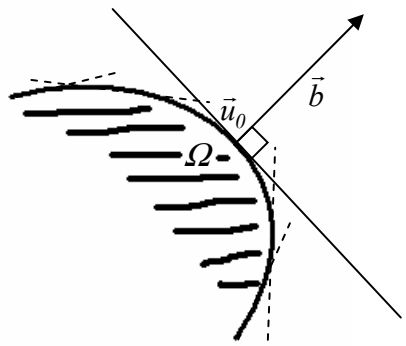

Figure 7: Choosing $\vec{u}_0^D$ at $\partial\Omega$ and $\vec{b}$ normal to $\partial\Omega$ defines a half-plane that Ω is bounded in. Repeating this for all points on $\partial\Omega$ encapsulates Ω, assuming that Ω is convex. The maximum principle implies that every convex set is invariant to the diffusion equation.

The uniqueness of the solution to the reaction-diffusion problem can be shown be a standard contradiction argument, however, this is omitted here (see [29] for reference).

3.1.4 Extension to the intial-boundary problem

The implications of adding boundary conditions of the type that describes the kinetochore turnover, called non-linear Robin conditions, to the initial value problem is a more difficult topic. A rigorous proof of existence of the initial-boundary problem (12)-(15) would demand more space than what is natural to include in a biological application setting, so the aim of this section will be to provide a clear indication that potentially problem-causing side effects that commonly arise when adding Robin boundary conditions are, in fact, insignificant in the wait-anaphase signal models.

Linear Robin boundary condition for symmetric systems of differential equations can be written

$$A\vec{u} \pm B\frac{\partial \vec{u}}{\partial \vec{n}} = C \text{ for } r \in R_K, R_C, \tag{25}$$

where A, B and C are matrices, here assumed to be constant. The normal derivative $\pm\frac{\partial \vec{u}}{\partial \vec{n}}$ is negative for R_K and positive for R_C. The three-component system defined in (17) is again used as test system, but now the kinetochore-bound reaction (10) is considered. Mathematically, the kinetochore turnover is described by the boundary conditions

$$-\begin{bmatrix} D_1 & 0 & 0 \\ 0 & D_2 & 0 \\ 0 & 0 & D_3 \end{bmatrix}\frac{\partial \vec{u}}{\partial \vec{n}} = \begin{bmatrix} J_\kappa \\ J_\kappa \\ -J_\kappa \end{bmatrix}. \tag{26}$$

The flux-vector which appears on the right-hand side of (26) is non-linear in $\vec{u}$. To investigate the impact of the boundary conditions on the solutions, the flux J_κ can be approximated by the first degree Taylor series

$$J_\kappa(\vec{u}) \approx J_\kappa(\vec{w}) + \sum_{i=1}^{3}\frac{\partial J_\kappa}{\partial u_i}\bigg|_{\vec{u}=\vec{w}} \Delta u_i = J_\kappa(\vec{w}) + j_k \ell_t \sum_{i=1}^{3}\frac{\partial \ell_C}{\partial u_i}\bigg|_{\vec{u}=\vec{w}} \Delta u_i \,,$$

for a fixed $\vec{w}$ and small $\Delta\vec{u} = \vec{u} - \vec{w}$. In matrix notation, the Taylor approximated flux-vector becomes

$$\begin{bmatrix} J_\kappa(\vec{u}) \\ J_\kappa(\vec{u}) \\ -J_\kappa(\vec{u}) \end{bmatrix} = \begin{bmatrix} J_\kappa(\vec{w}) \\ J_\kappa(\vec{w}) \\ -J_\kappa(\vec{w}) \end{bmatrix} + j_\kappa \ell_t \left[\begin{matrix} \frac{\partial \ell_C}{\partial u_1} & \frac{\partial \ell_C}{\partial u_2} & \frac{\partial \ell_C}{\partial u_3} \\ \frac{\partial \ell_C}{\partial u_1} & \frac{\partial \ell_C}{\partial u_2} & \frac{\partial \ell_C}{\partial u_3} \\ -\frac{\partial \ell_C}{\partial u_1} & -\frac{\partial \ell_C}{\partial u_2} & -\frac{\partial \ell_C}{\partial u_3} \end{matrix} \right]_{\vec{u}=\vec{w}} \Delta\vec{u} \,. \tag{27}$$

The boundary conditions are linearized by replacing the right-hand side in (26) with the Taylor approximation (27), which yields

$$\underbrace{j_\kappa \ell_t \left[\begin{matrix} \frac{\partial \ell_C}{\partial u_1} & \frac{\partial \ell_C}{\partial u_2} & \frac{\partial \ell_C}{\partial u_3} \\ \frac{\partial \ell_C}{\partial u_1} & \frac{\partial \ell_C}{\partial u_2} & \frac{\partial \ell_C}{\partial u_3} \\ -\frac{\partial \ell_C}{\partial u_1} & -\frac{\partial \ell_C}{\partial u_2} & -\frac{\partial \ell_C}{\partial u_3} \end{matrix} \right]_{\vec{u}=\vec{w}}}_{A} \vec{u} + \overbrace{\begin{bmatrix} -D_1 & 0 & 0 \\ 0 & -D_2 & 0 \\ 0 & 0 & -D_3 \end{bmatrix}}^{B} \frac{\partial \vec{u}}{\partial \vec{n}} =$$

$$\underbrace{\begin{bmatrix} J_\kappa(\vec{w}) \\ J_\kappa(\vec{w}) \\ -J_\kappa(\vec{w}) \end{bmatrix} + j_\kappa \ell_t \left[\begin{matrix} \frac{\partial \ell_C}{\partial u_1} & \frac{\partial \ell_C}{\partial u_2} & \frac{\partial \ell_C}{\partial u_3} \\ \frac{\partial \ell_C}{\partial u_1} & \frac{\partial \ell_C}{\partial u_2} & \frac{\partial \ell_C}{\partial u_3} \\ -\frac{\partial \ell_C}{\partial u_1} & -\frac{\partial \ell_C}{\partial u_2} & -\frac{\partial \ell_C}{\partial u_3} \end{matrix} \right]_{\vec{u}=\vec{w}}}_{C} \vec{w} \,. \tag{28}$$

For a one-dimensional system, A and B are scalars. In the scalar case, if A and B have opposite signs, the boundary conditions will function as a negative feedback loop. Equal signs will, on the contrary, result in positive feedback loop. A positive feedback can cause blow-ups in the solutions, while a negative feedback loop is generally regarded a stabilizing mechanism. To ensure that the boundary conditions (26) do not cause blow-ups in the solutions of the reaction-diffusion system, restrictions must be imposed on the matrices A and B in (28). For an N-dimensional system the negative feedback is guaranteed if the matrix $A^{-1}B$ or, equivalently, $B^{-1}A$ has exclusively non-positive eigenvalues.

The partial derivatives in (28) are given by

$$\frac{\partial \ell_C}{\partial u_i} = \begin{cases} u_2 e^{-u_1 u_2}, & i = 1 \\ u_1 e^{-u_1 u_2}, & i = 2 \\ 0, & i = 3 \end{cases}. \tag{29}$$

By substituting (29) in (28), $B^{-1}A$ can be computed,

$$B^{-1}A = -j_\kappa \ell_t \begin{bmatrix} \frac{1}{D_1} & 0 & 0 \\ 0 & \frac{1}{D_2} & 0 \\ 0 & 0 & \frac{1}{D_3} \end{bmatrix} \begin{bmatrix} w_1 e^{-v_1 v_2} & w_2 e^{-v_1 v_2} & 0 \\ w_1 e^{-v_1 v_2} & w_2 e^{-v_1 v_2} & 0 \\ -w_1 e^{-v_1 v_2} & -w_2 e^{-v_1 v_2} & 0 \end{bmatrix} = j_\kappa \ell_t \begin{bmatrix} -\frac{w_1 e^{-w_1 w_2}}{D_1} & -\frac{w_2 e^{-w_1 w_2}}{D_1} & 0 \\ -\frac{w_1 e^{-w_1 w_2}}{D_2} & -\frac{w_2 e^{-w_1 w_2}}{D_2} & 0 \\ \frac{w_1 e^{-w_1 w_2}}{D_3} & \frac{w_2 e^{-w_1 w_2}}{D_3} & 0 \end{bmatrix}.$$

$B^{-1}A$ is clearly of rank one and has therefore only one eigenvalue. Since the trace is negative and the sum of eigenvalues is equal to the trace, the eigenvalue is itself negative. It is therefore safe to conclude that adding the specified boundary conditions will provide the system with a negative feedback loop.

3.2 Assessing model parameters

3.2.1 Measurement techniques

Conclusions concerning a biological system that are based on simulation results of a mathematical model will naturally dependent to a large extent on the parameter values used. To ensure that the simulated data is relevant to the biological system, it is fundamental to have a realistic set of parameter values. An intra-cellular signal transduction network can involve tens or hundreds of molecular species, that each typically gives raise to a variable in the corresponding mathematical model. In a reaction-diffusion model, the number of parameters is at least the same as the number of variables. In a biochemical setting the number of parameters typically exceeds the number of variables by about 2-3 fold, so 50 parameters or more is not unusual. On the other hand are biological assays to measure these parameters often inaccurate, time-consuming and expensive, especially when performing quantitative measurements. As an example relevant to the work presented here; performing rate measurements that would support or reject the hypothesized deactivation of p31 at unattached kinetochores could consume many months of hard work by highly trained personnel and deep cuts in laboratory budgets. Therefore, due to the resources that are demanded, it is rarely possible to build a model based solely on measured parameters. The parameters that cannot be measured must be filled in by estimates, standard or measured values in the literature or educated guesses based on analogous reactions in other biochemical systems.

In the mathematical modeling framework described in Ch 3.1, three main categories of parameters are introduced: protein concentrations, diffusion constants and reaction rates. The reaction rates can be divided into three sub-categories: cytoplasmic association rates, cytoplasmic dissociation rates and kinetochore turn-over rates. In addition to these are the geometrical and temporal parameters of the model, which describe the spatio-temporal domain that the reaction-diffusion equations are solved over. To obtain a full set of parameter values, results from a variety of laboratory assays, generalized results or assumptions must be utilized, as discussed in Ch. 3.2.2-3.2.5.

3.2.2 Cytoplasmic rates

A forward type reaction describes the binding of two substrates to form a product, as defined in (8). The cytoplasmic forward reactions defined in the biological models in Ch.2 can all be assumed to be diffusion limited, which means that when the substrates meet, they will bind [31]. This implies that the rate of the reaction is limited by the rate at which the substrates collide and not the molecular species ability to bind when they meet per se. Diffusion limited reactions are, therefore, considered the fastest reactions that can theoretically occur in a reaction-diffusion system [19].

A reverse reaction describes the dissociation of a product to its original substrates (9). The dissociation rates cannot be assessed by a general assumption, like in the case of association rates, since the molecular complexes that appear in the system have different stability properties that determine their life-time.

Central in the core-circuitry is the rate at which the inhibited APC-MCC-complex dissociates after complete kinetochore attachment. This rate is measured by an advanced microscopy method called Fluorescence Correlation Spectroscopy (FCS). FCS detects fluctuations of fluorescence intensity in a small excitation volume of approximately $0.1\ fL$ that are caused by the Brownian motion of the fluorescently tagged molecules in the cytoplasm. For every observation interval, the auto-correlation function of the sampled fluorescence intensity is calculated and used to infer information about the dynamics of the tagged species (Figure 8a). In the first instance, FCS provides information about diffusion constants and protein concentrations. Fast dynamics indicate a short residence time in the excitation volume and a large diffusion coefficient, whereas slow dynamics indicate the opposite. Concentrations are derived directly from the intensity data. Combining FCS data from several sample times provides the temporal change in protein concentrations and diffusion constant, and an indirect measure of the dissociations rate (Figure 8b).

Other dissociation rates in the mathematical models are assessed by various methods. A brief indication to what assays are used to obtain the full set of parameter values are given is Table 3 in Ch. 4.

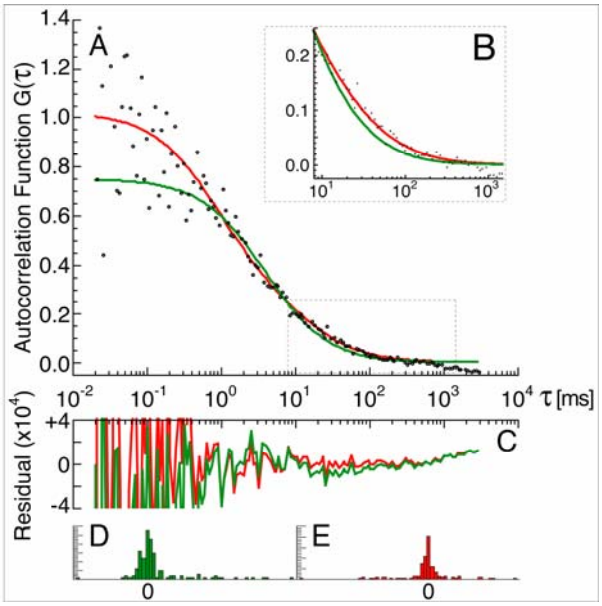

Figure 8a: The black dots (A) represent the normalized sample correlation function G(τ) calculated from the FCS data. A single-component (green) and a two-component (red) least-squares fit are shown, with respective residuals (C). The two-component regression provides a better fit, especially in the 10-100 ms region (B), and a more symmetric residual distribution (D and E). The rationale behind the superiority of the two-component fit is that Mad2 is both bound in a small complex and a large complex (MCC and APC/C-MCC) and that these have different kinetics.

Figure credits: Jagesh V. Shah, Harvard Medical School.

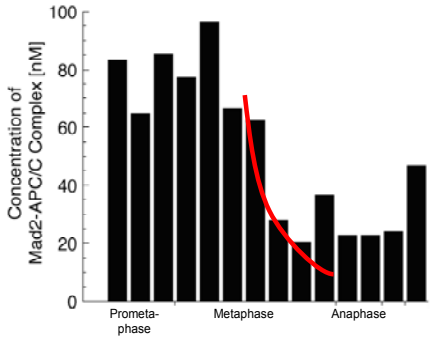

Figure 8b: The concentration of the APC/C-MCC complex can be measured by FCS. In metaphase, a significant drop in concentration of inhibited APC/C-MCC is observed, followed by anaphase approximately 10 minutes later. The bars are 3 minutes apart. The red line indicates how an exponential decay can be fitted to the data, which provide a measurement of the dissociation rate of APC-MCC.

Figure credits: Jagesh V. Shah, Harvard Medical School.

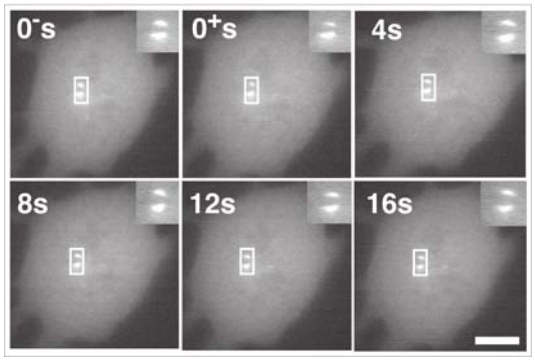

Figure 9: FRAP data from an experiment where p31 dynamics at the kinetochore is investigated. At time 0s the upper kinetochore is bleached by a non-damaging laser pulse that causes a reduction of fluorescence intensity (0^-s and 0^+s). The fluorescence intensity of the kinetochore is then sampled every second. The recovery rate of the kinetochore fluorescence intensity is interpreted as the turnover rate of p31 and the production rate of p31*.

Figure credits: Michael S. Manak, Harvard Medical School.

3.2.3 Kinetochore turnover rates

The turnover rates of protein species at the kinetochores can be measured by another advanced microscopy technique called Fluorescence Recovery After Photobleaching (FRAP). As with FCS, FRAP can monitor the dynamics of fluorescently tagged protein in vivo. The wait-anaphase signal is known to be emitted from binding sites at unattached kinetochores. By fluorescently tagging the proteins that are turning over, the signaling kinetochores are illuminated more than the background when observed under a fluorescent microscope, due to an enrichment of tagged protein species. The illuminated kinetochores are then bleached by the use of a short laser pulse. Since the bleaching does not alter kinetochore turnover, illumination is recovered as bleached protein is replaced by cytoplasmic unbleached protein that enters the kinetochore binding sites (Figure 9). The half-recovery time in fluorescence recovery provides a measure of the rate at which kinetochores are producing the wait-anaphase signal. Together with an estimate of the number of MCC-molecules that are present at a single kinetochore, the protein flux that the kinetochore-bound reaction imposes can be assessed.

3.2.4 Protein concentrations and diffusion constants

As described in Ch. 3.2.2, diffusion constants can be measured by counting to number of molecules that visit a small excitation volume by FCS. Since the excitation volume is known, the concentration of the species can easily be calculated. FCS measurements demand large resources and are at the current rarely applied for the sole purpose of measuring protein concentrations. A more typical method is to measure protein concentrations by biochemical immunoassays, which are based on the use of antibodies. Antibodies are central in the vertebrate immune system since they can identify foreign microorganisms such as viruses and bacteria. In immunoassays, the ability to recognize specific molecular motifs is utilized to show the presence and measure the concentration of proteins.

An important limitation of most biochemical assays is that they only provide bulk measurements of protein levels, not directly compatible with the high resolution in parameters which appear in the mathematical models of the wait-anaphase signal. The signal component Mad2, as an illustrative example, is present in several different states; i.e., the pure forms O-Mad2 and C-Mad2 and the complex states MCC, MCC-p31, APC-MCC and APC-MCC-p31. In the biological models, the concentration of each individual Mad2-containing species is described in space and time. In fact, simulating the models will demand that all molecular species are specified with a spatial profile at a fixed time in the initial conditions. This level of detail is not met be the biological assays, which can only provide bulk measurements of total concentrations, independent of the state it is in, without any spatial information, and maybe averaged over millions of cells.

Obviously, there is a gap between the information laboratory measurements can be expected to provide about protein concentrations and the initial conditions needed to run numerical simulations of the mathematical model. This gap can be filled by introducing further assumptions about the system, but this discussion is left for Ch. 4.2.3.

3.3 Simulations

3.3.1 Computational framework

A computational framework to solve systems of reaction-diffusion equations was implemented in MATLAB. The central component of the program is the pre-defined *pdepe*-function, which solves initial-boundary systems of parabolic and elliptic partial differential equations numerically in one spatial dimension and time. A set of canonical parameter values are used as input, either directly in a single simulation or as a series of systematically modulated simulations, as in sensitivity or robustness analyses (Figure 10).

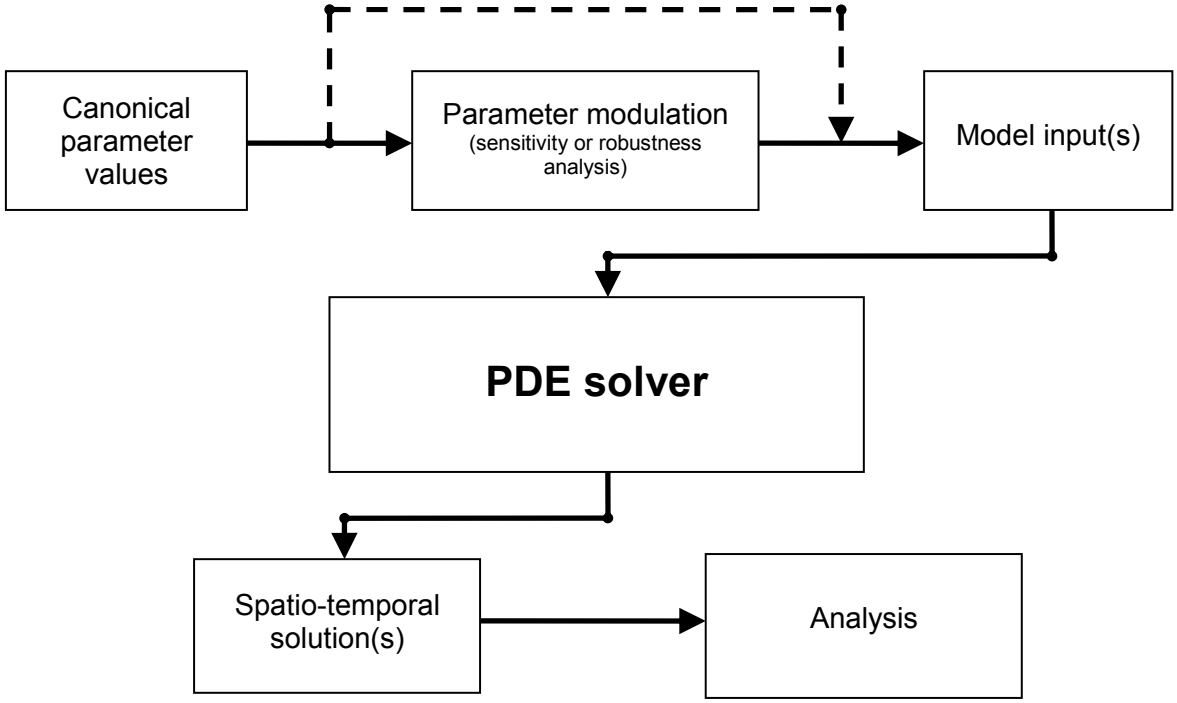

Figure 10: A schematic representation of the computational framework used to simulate the different mitotic checkpoint signaling mechanisms. The core component of the framework is a partial differential equation (PDE) solver. The solver is provided an input of canonical parameter values, possibly modulated to perform a sensitivity or robustness analysis. The solutions simulate protein concentrations in space and time and are used to analyze mitotic checkpoint signaling.

3.3.2 Orchestra computational cluster

Several of the results presented in Ch. 5 are based on repeated simulations of the biological models with modulated parameter values. Large scale simulations with 100 or more simulations consume significant computer power, enough to sequester a fast PC for several days. Therefore, large jobs are submitted to the Orchestra computing cluster at Harvard Medical School. The system has available 162 3GHz computational nodes and can run parallel simulations of the MATLAB framework, something that considerably reduce computation time.

4 Mathematical models

Chapter summary:

The biological models introduced in Chapter 2 and the mathematical theory and parameter assessments presented in Chapter 3 are merged in a simple geometric model of a single mammalian cell. A set of 15 reaction-diffusion equations, with specified initial-boundary conditions, are formulated. The mathematical models simulate the essential physico-chemical properties of the wait-anaphase signal.

4.1 Physico-chemical modeling framework

4.1.1 Modeling basics and geometry

The number of chromosomes that must obtain bipolar attachments before the wait-anaphase signal source completely disappears varies from species to species. Humans, as an example, have 46. The critical point of the mitotic checkpoint system is the ability to maintain checkpoint arrest when a single kinetochore is unattached, without altering the ability to rapidly release once the final attachment is made. All mammalian cells and most eukaryotes[1] are dependent on the ability of the last kinetochore to communicate throughout the entire cell that chromosome segregation is premature. It is reasonable to assume that if a single unattached kinetochore can solely provide tight APC/C inhibition, more the one kinetochore can also. A generic model constructed for investigating the ability of the mitotic checkpoint wait-anaphase signal to both tightly inhibit and rapidly release should therefore be focused on the performance of the last unattached kinetochore.

Mammalian kinetochores are disk-shaped structures with an approximated diameter of *200nm* [33,34]. The kinetochores are equipped with binding sites that modify several cytoplasmic proteins and thereby emit the mitotic checkpoint wait-anaphase signal. The details of the kinetochore-bound reactions are indeed important and interesting when

[1] A recent publication claims that Drosophila-cells (i.e., cells from fruit flies) undergo normal and healthy mitosis without need of the mitotic checkpoint [32]. Yeast cells can also divide and survive for a significant time without a functional mitotic checkpoint.

investigating to the mitotic checkpoint. However, in the biological models of the various signaling mechanisms introduced in Ch. 2 only the net results (i.e. what goes in and what comes out) of the kinetochore turnover process is directly relevant. The kinetochore flux can, therefore, conveniently be parameterized by defining a spatial compartment called the "kinetochore-region"; a centrally located spherical region that encapsulates the last unattached kinetochore. The kinetochore turnover can then be modeled by the flux of cytoplasmic protein that is imposed over the boundary of the kinetochore-region. The geometry of the cell itself can also be assumed to be spherical, since most mammalian cells contract into a nearly spherical shape in mitosis. The diameter of a mitotic mammalian cells is variable, but most are within a range of *10-20μm* [35]. A suitable geometric setup for modeling the mitotic checkpoint is, therefore, obtained by embedding the kinetochore-region in the much larger, also spherical, cell geometry. The volume between the kinetochore-region and the outer boundary of the cell model is named the cytoplasmic-region. The cytoplasmic signaling network is modeled by a set of reaction-diffusion equations in the cytoplasmic region (Figure 11). A similar modeling setup was introduced in a recent pioneering paper [36]; however, the results are limited to the mitotic checkpoint in yeast.

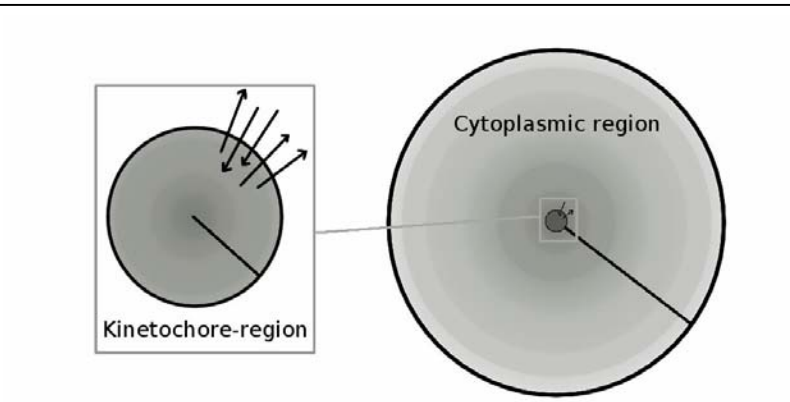

Figure 11: The kinetochore-region is fictive sphere of radius *100nm*, that encapsulates the last unattached kinetochore. The cytoplasmic region is also sphere-shaped, covering the volume between the kinetochore-region and the outer boundary pf the cell. The outer boundary of the cell is modeled as a spherical shell of radius *9μm*. The kinetochore-region is centrally located in the cytoplasmic region. The kinetochore-bound reactions are connected to the cytoplasmic interaction network through a flux over the cytoplasm-kinetochore-boundary. The cytoplasmic interaction network is modeled as a set of reaction-diffusion equations in the cytoplasmic region.

4.1.2 Temporal modeling interval

Before proper spindle attachments are made the cytoplasm is scanned for unattached kinetochores by a biased random walk of the microtubules ends [37]. Due to the randomness of the microtubule search-and-capture process, the time of complete kinetochore attachment to the mitotic spindle is a stochastic variable. However, the generic modeling setup introduced in Ch. 4.1.1 leaves out the attachment process of all kinetochores but the very last. The temporal modeling interval can, therefore, be chosen around the event of complete kinetochore attachment, regardless of the stochastic nature of its occurrence.

The kinetochore attachment process can last for several hours, where the waiting for the last kinetochore is calculated to consume as much as 25% of the total search-and-capture time [36]. Because the significant time a single kinetochore is likely to operate alone, it can assumed that the chemical reactions that compose the wait-anaphase signal are in steady-state, or at least close to steady-state, at the time of complete kinetochore attachment. Consequently, the reaction-diffusion system should be allowed to reach steady-state with one kinetochore unattached before complete kinetochore attachment occurs.

The temporal modeling interval can therefore be defined to start at the time of complete kinetochore attachment, assuming steady-state in cytoplasmic reactions. The response in the cytoplasmic interaction network to silencing of the final kinetochore should not last longer then the longest observed time from complete kinetochore attachment to anaphase initiation, which is approximately 45 minutes [5]. A 60 minute modeling interval is therefore an appropriate choice. The time of complete kinetochore attachment is denoted t_1 and the end of the modeling interval t_2, where $t_2 = t_1 + \Delta t$ and Δt is 60 minutes.

4.1.3 Notation and summary of the biological models

The biological models of the wait-anaphase signal involve $N=15$ molecular species, summarized in Table 1. All concentrations are gathered in a vector notation,

$$\vec{u} = [m, m^*, m' m^p, c, c^*, b, b^c, p, p^*, a, a^*, a^p, a^c, s] \equiv [u_1, \ldots u_{15}]$$

where the components are functions of space and time,

$$u_i = u_i(\vec{r}, t) \text{ for } i=1 \ldots 15.$$

The geometry, the diffusion process and the reactions of the models are spherically

symmetric, a property that is inherited by the solutions of the reaction-diffusion equations:

$$u_i = u_i(r,t) \text{ for } i=1\ldots15.$$

where $r = |\vec{r}|$.

The reactions that the molecular species are involved in are summarized in Table 2.

Species	*Symbol*	*Description*	*Notes*
Mad2	m	Pure Mad2	
MCC	$m*$	Mad2-BubR1-Cdc20-complex	Known as the Mitotic Checkpoint Complex (MCC)
MCC´	m'	Inactive MCC	
MCC-p31	m^p	MCC bound to p31	
Cdc20	c	Pure Cdc20	Able to activate APC/C
Cdc20*	$c*$	Inactivated Cdc20	Unable to activate APC/C
BubR1	b	Pure BubR1	
BubR1-Cdc20	b^c	BubR1-Cdc20 complex	
p31	p	Pure p31comet	Able to catalyze APC/C-MCC disassembly
p31*	$p*$	Inactive p31comet	Unable to catalyze APC/C-MCC disassembly
APC/C	a	The Anaphase-Promoting Complex	Unable to degrade Securin
APC/C-MCC	$a*$	APC/C inhibited by MCC	Unable to degrade Securin
APC/C-MCC-p31	a^p	APC/C-MCC bound to p31	Unable to degrade Securin
APC/C-Cdc20	a^c	Active APC/C	Able to degrade Securin
Securin	s	The pool of Securin left in the system	

Table 1: The molecular species introduced by the biological models.

Process	*Reaction*	*Spatial location*	*Models*
MCC formation	$m + b^c \xrightarrow{\mu} m*$	Unattached kinetochores	Kinetochore MCC assembly
MCC activation	$m' \xrightarrow{\mu} m*$	Unattached kinetochores	Cytoplasmic MCC assembly
p31 inactivation	$p \xrightarrow{\sigma} p*$	Unattached kinetochores	Complex wait-anaphase signal
Cdc20 inactivation	$c \xrightarrow{\gamma} c*$	Kinetochores	Cdc20 buffering
Spontaneous MCC dissociation	$m* \xrightarrow{\bar{\mu}} m + b + c$	Cytoplasm	All
p31 reactivation	$p* \xrightarrow{\bar{\sigma}} p$	Cytoplasm	Complex wait-anaphase signal
Cdc20 reactivation	$c* \xrightarrow{\bar{\gamma}} c$	Cytoplasm	Cdc20 buffering
BubR1-Cdc20 complex formation	$b + c \underset{\bar{\beta}^c}{\overset{\beta^c}{\rightleftarrows}} b^c$	Cytoplasm	All
Cytoplasmic MCC formation	$m + b^c \underset{\bar{\beta}^c}{\overset{\beta^c}{\rightleftarrows}} m'$	Cytoplasm	Kinetochore MCC assembly
MCC-p31 complex formation	$m* + p \underset{\bar{\alpha}^p}{\overset{\alpha^p}{\rightleftarrows}} m^p$	Cytoplasm	All
MCC amplification	$m* + m + b^c \xrightarrow{\mu_{amp}} 2m*$	Cytoplasm	MCC amplification
APC/C-MCC-complex formation	$a + m* \underset{\bar{\alpha}*}{\overset{\alpha*}{\rightleftarrows}} a*$	Cytoplasm	All
APC/C-MCC-p31-complex formation	$\left.\begin{array}{l} a* + p \underset{\bar{\alpha}^p}{\overset{\alpha^p}{\rightleftarrows}} \\ a + m^p \underset{\bar{\alpha}*}{\overset{\alpha*}{\rightleftarrows}} \end{array}\right\} a^p \xrightarrow{\bar{\alpha}} a + m + b + c + p$	Cytoplasm	All
APC/C activation	$a + c \underset{\bar{\alpha}^c}{\overset{\alpha^c}{\rightleftarrows}} a^c$	Cytoplasm	All
Securin degradation	$a^c + s \xrightarrow{\lambda} a^c + \varnothing$	Cytoplasm	All

Table 2: Molecular reactions introduced by the biological models.

4.2 Reaction-diffusion model specification

4.2.1 Cytoplasmic reactions and diffusion

The chemical reactions gathered in Table 2 define the cytoplasmic part of the mitotic checkpoint wait-anaphase signaling network. By applying the mathematical theory presented in Ch. 3.1 to these reactions, the following set of reaction-diffusion equations is obtained:

$$\frac{\partial m}{\partial t} = D_m \Delta_r m + \bar{\mu} m^* + \bar{\alpha}^* a^* + \bar{\alpha}^p a^p - \mu' m b^c + \bar{\mu}' m' - \mu_{amp} m^* m b^c \tag{30}$$

$$\frac{\partial m^*}{\partial t} = D_{m^*} \Delta_r m^* - \bar{\mu} m^* - \mu^p m^* p + \bar{\mu}^p m^p - \alpha^* a m^* + \mu_{amp} m^* m b^c \tag{31}$$

$$\frac{dm'}{dt} = D_{m'} \Delta_r m' + \mu' m b^c - \bar{\mu}' m' \tag{32}$$

$$\frac{\partial m^p}{\partial t} = D_{m^p} \Delta_r m^p + \mu^p m^* p - \bar{\mu}^p m^p - \alpha^* a m^p + \bar{\alpha}^* a^p \tag{33}$$

$$\frac{\partial c}{\partial t} = D_c \Delta_r c + \bar{\mu} m^* - \beta b c + \bar{\beta} b^c + \bar{\alpha}^* a^* + \bar{\alpha}^p a^p - \alpha^c a c + \bar{\alpha}^c a^c + \bar{\gamma} c^* \tag{34}$$

$$\frac{\partial c^*}{\partial t} = D_{c^*} \Delta_r c^* - \bar{\gamma} c^* \tag{35}$$

$$\frac{\partial b}{\partial t} = D_b \Delta_r b + \bar{\mu} m^* - \beta b c + \bar{\beta} b^c + \bar{\alpha}^* a^* + \bar{\alpha}^p a^p \tag{36}$$

$$\frac{\partial b^c}{\partial t} = D_{b^c} \Delta_r b^c + \beta b c - \bar{\beta} b^c - \mu' m b^c + \bar{\mu}' m' - \mu_{amp} m^* m b^c \tag{37}$$

$$\frac{\partial p}{\partial t} = D_p \Delta_r p - \mu^p m^* p + \bar{\mu}^p m^p - \mu^p a^* p + \bar{\mu}^p a^p + \bar{\alpha}^p a^p + \bar{\sigma} p^* \tag{38}$$

$$\frac{\partial p^*}{\partial t} = D_{p^*} \Delta_r p^* - \bar{\sigma} p^* \tag{39}$$

$$\frac{\partial a}{\partial t} = D_a \Delta_r a - \alpha^* a m^* + \bar{\alpha}^* a^* - \alpha^* a m^p + \bar{\alpha}^* a^p + \bar{\alpha}^p a^p - \alpha^c a c + \bar{\alpha}^c a^c \tag{40}$$

$$\frac{\partial a^*}{\partial t} = D_{a^*} \Delta_r a^* + \alpha^* a m^* - \bar{\alpha}^* a^* - \mu^p a^* p + \bar{\mu}^p a^p \tag{41}$$

$$\frac{\partial a^p}{\partial t} = D_{a^p} \Delta_r a^p + \mu^p a^* p - \bar{\mu}^p a^p + \alpha^* a m^p - \bar{\alpha}^* a^p - \bar{\alpha}^p a^p \tag{42}$$

$$\frac{\partial a^c}{\partial t} = D_{a^c} \Delta_r a^c + \alpha^c a c - \bar{\alpha}^c a^c \tag{43}$$

$$\frac{\partial s}{\partial t} = D_s \Delta_r s - \lambda a^c s \tag{44}$$

Terms encapsulated in red boxes correspond to the cytoplasmic MCC assembly model and are excluded in other models. Likewise, the terms in blue boxes belong to the cytoplasmic MCC amplification model, green boxes to the Cdc20-buffering pathway and yellow boxes to the p31 inactivation pathway in the complex wait-anaphase signal model.

4.2.2 Kinetochore flux and boundary conditions

The biological models suggest three parallel kinetochore turnover processes: MCC production and p31 and Cdc20 inactivation. Naturally, for the production of MCC, p31* and Cdc20* to take place the substrates of the reactions must be transported to the kinetochore and the products transported away. Hence, the kinetochore turnover processes imposes protein fluxes in and out of the kinetochore region. In the mathematical framework these fluxes are included through special boundary conditions,

$$-D_i \frac{\partial u_i}{\partial \vec{n}} = J_i \quad \text{for } i=1\ldots15, \tag{45}$$

where $\vec{n}$ if unit normal to the kinetochore-region and J_i is the flux density corresponding to the i'th component in $\vec{u}$. The protein flux functions are defined in Ch. 3.1.1 as

$$J_i = J_i(\vec{u},t) = j_i \cdot \ell_C \cdot \ell_t \quad \text{for } i=1\ldots15, \tag{46}$$

where j_i is the flux density at maximal kinetochore turnover and $\ell_C, \ell_t \in [0,1]$ are regulatory functions that silence the wait-anaphase signal according to spindle attachment and lack of substrate, respectively. Assigning to each component in $\vec{u}$ the flux imposed by the turnover of MCC, p31* and Cdc20* yields

$$\vec{j} = [\, j_1,\ldots,j_N \,] = [\underbrace{-j_\mu}_{MCC}, j_\mu, -j_\mu, 0, \overbrace{-j_\gamma, j_\gamma}^{Cdc20*}, 0, \underbrace{-j_\mu}_{MCC}, \overbrace{-j_\sigma, j_\sigma}^{p31*}, 0,0,0,0,0] \,. \tag{47}$$

Red solid box indicates the substrate flux imposed by the activation of MCC in the cytoplasmic MCC assembly model, while red dotted boxes indicate the substrate flux in the core-circuitry. In such, the fluxes in the red solid box and the red dotted boxes are exclusive. The green and yellow boxes indicates the fluxes imposed by the Cdc20* and p31* turnover processes.

The kinetochore turnover rates μ, γ and σ can be defined with units s^{-1} (molecules per

sec). The maximal kinetochore fluxes imposed by production of MCC, p31* and Cdc20* can be expressed by the rates of the kinetochore-bound reactions

$$j_\mu = \frac{k\mu}{A_{R_K}}, j_\sigma = \frac{k\sigma}{A_{R_K}}, j_\gamma = \frac{k\gamma}{A_{R_K}}, \tag{48}$$

where $A_{R_K} = 4\pi R_K^2$ is the surface area of the kinetochore-region. The scaling constant k couples the units of the turnover parameters to the units of the boundary conditions:

$$[\mu] = [\sigma] = [\gamma] = s^{-1} = \frac{dm^3 \cdot nmol}{dm^3 \cdot nmol} s^{-1} = \frac{10^{24}}{6.022 \cdot 10^{14}} \frac{nm^3 \cdot nmol}{s \cdot L} = 1.661 \cdot 10^9 \frac{nm^3 \cdot nM}{s},$$

which yields $k = 1.661 \cdot 10^9 nm^3 nM$.

At the outer boundary of the cell model there is no protein flux,

$$-D_i \frac{\partial u_i}{\partial \vec{n}} = 0 \text{ for } i=1...15. \tag{49}$$

The boundary conditions that describe the formation of MCC, Cdc20* and p31* at kinetochores are given by (45)-(48). The outer boundary conditions are defined by (49). The full boundary condition for the system is simply defined by adding together the kinetochore-cytoplasm boundary flux and the zero-flux outer boundary conditions.

4.2.3 Initial conditions

As stated in Ch. 3.2.4, biological assays can normally only provide bulk measurements of protein concentrations. To obtain accurate level measurements or detailed information about a spatial protein gradient in single cells is unrealistic at the present time. On the other hand, in order to run simulations of the reaction-diffusion models, initial concentration profiles of all molecular species must be specified.

Despite the discrepancy in available concentration measurements and initial concentration profiles needed in the mathematical model, useful information can be extracted from the measured values to construct initial conditions that represent the cellular conditions. The "total concentration" of Mad2 can be defined as the sum of the spatial concentration averages of all Mad2-containing species:

$$m_{TOT} = \overline{m} + \overline{m}^{*} + \overline{m}' + \overline{m}^{p} + \overline{a}^{*} + \overline{a}^{p} \tag{50}$$

Likewise, can the total concentration of Cdc20, BubR1, p31 and APC/C be defined as:

$$c_{TOT} = \overline{m}^{*} + \overline{m}' + \overline{m}^{p} + \overline{c} + \overline{c}^{*} + \overline{b}^{c} + \overline{a}^{*} + \overline{a}^{p} + \overline{a}^{c}, \tag{51}$$

$$b_{TOT} = \overline{m}^{*} + \overline{m}' + \overline{m}^{p} + \overline{b} + \overline{b}^{c} + \overline{a}^{*} + \overline{a}^{p}, \tag{52}$$

$$p_{TOT} = \overline{m}^{p} + \overline{p} + \overline{p}^{*} + \overline{a}^{p}, \tag{53}$$

$$a_{TOT} = \overline{a} + \overline{a}^{*} + \overline{a}^{p} + \overline{a}^{c}. \tag{54}$$

The bars in (50)-(54) indicate the spatial mean over the cytoplasmic region $R_K < r < R_C$. The total concentrations are gathered in vector notation

$$\vec{v} = [m_{TOT}, c_{TOT}, b_{TOT}, p_{TOT}, a_{TOT}].$$

The vector $\vec{v}$ can be assumed to be measurable by the use of a variety of biological measurement techniques. By construction, a measured vector $\vec{v} = \vec{v}^{0}$ corresponds to an infinite number of initial concentration profiles $\vec{u}^{0}(r) = \vec{u}(r, t_0)$, since the distribution of Mad2, Cdc20, BubR1, p31 and APC/C into the 15 molecular species in $\vec{u}$ and the spatial profile of these is not specified. The time t_0 is defined as $t_0 = t_1 - \Delta t$, where Δt is sufficiently large for steady-state to be reached at time t_1.

The mathematical simulation framework is constructed for the purpose of investigating single kinetochore ability to maintain checkpoint arrest and allow rapid release. The ability to arrest properly is analyzed by considering the system steady-state degradation of Securin at the time of complete kinetochore attachment. The behavior of the reaction-diffusion system before steady-state is reached is of no particular interest in this regard. This suggests that the relationship between a fixed vector $\vec{v} = \vec{v}^{0}$ and the steady-state profiles at the time of complete kinetochore attachment,

$$\vec{u}^{SS}(r) = \vec{u}(r, t_1),$$

should be investigated.

An attractive possibility is that there is precisely one steady-state profile that corresponds to every fixed total concentration vector. This would indicate that the steady-state concentration $\vec{u}^{SS}$ is indifferent to the choice of initial conditions $\vec{u}^{0}$, as long as $\vec{v}$ is fixed,

something that would dwindle the gap between measurements and mathematics significantly. A strong indication that there, in fact, is a one-to-one relationship between $\vec{v} = \vec{v}^0$ and $\vec{u}^{SS}$ can be provided by a fairly straight forward computational investigation. The total concentrations (50)-(54) defines a hyper-plane in $\Re^{15}$. A point on this hyper-plane is a valid distribution of the total concentrations $\vec{v}$ into the 15 molecular species contained in $\vec{u}$ that correspond to a measured vector $\vec{v}^0$. To test if all such valid distributions map to a unique steady-state profile $\vec{u}^{SS}$, 10 000 samples were drawn from the hyper-plane (50)-(54) by a random walk procedure. Simulations of the wait-anaphase models were carried out, with these samples used as uniform initial conditions. All simulations displayed the same steady-state concentration profile, within a small error threshold. This result strongly indicates that the steady-state profile $\vec{u}^{SS}$ is invariant to the distribution of the initial conditions, as long as $\vec{v}$ is constant.

4.2.4 Parameter values

The mathematical models of the wait-anaphase signal introduce a number of parameters that are assessed using a variety of general results and measurement techniques, as discussed in Ch. 3.2.

For simplicity can the diffusion of molecular species be roughly divided into two categories, i.e., fast and slow. This is reasonable since the APC/C is much larger in molecular size then the other species in the system. In such, the slow diffusing molecules in the system are defined as the APC/C-containing and the fast diffusing molecules are defined as the non-APC/C-containing. Corresponding diffusion constants are measured by FCS to be $D_{fast} = 18\mu m^2 s^{-1}$ and $D_{slow} = 1\mu m^2 s^{-1}$ [38].

A measurement of the MCC turnover indicates that approximately 100 molecules are produced at a single kinetochore per second, a measurement based on the half-recovery time of tagged Mad2, together with Mad2 occupancy data, at the kinetochores [17,18]. By similar means is the inactivation rates of p31 and Cdc20 at the kinetochores estimated to be 500 molecules per second [17,18,23].

All association rates are assumed to be diffusion limited. The canonical value for diffusion limited reaction in biological systems is *1nM* [19]. Dissociation rates are found by a combination of methods. A central parameter is the degradation of APC/C-MCC in anaphase, which is measured to occur at a rate of *0.0013/s* [38].

Total concentrations of Mad2, Cdc20, BuBR1, p31 and APC are extracted from several publications [10,11,15], with values *100nM*, *120nM*, *120nM*, *200nM* and *80nM* respectively.

The full set of parameter values, hereafter denoted the canonical parameters, are gathered in Table 3.

Description	*Symbol(s)*	*Value/units*	*Method/source*	*Reference*
Fast diffusion	D_{fast}	$18\mu m^2 s^{-1}$	FCS measurement	[38]
Slow diffusion	D_{slow}	$1\mu m^2 s^{-1}$	FCS measurement	[38]
MCC production rate	μ	$100s^{-1}$	FRAP measurement	[17,18]
p31* production rate	σ	$500s^{-1}$	FRAP measurement/ Estimate	[17,18,23]
Cdc20* production rate	γ	$500s^{-1}$	FRAP measurement/ Estimate	[17,18,23]
Complex formation rate (association)	$\mu', \beta^c, \alpha^p, \alpha^*, \alpha^c$	$1s^{-1}nM^{-1}$	Diffusion limited rate, literature value	[19]
MCC spontaneous dissociation	$\overline{\mu}, \overline{\mu}'$	$0.001s^{-1}$	Estimated	
p31 reactivation	$\overline{\sigma}$	$0.005s^{-1}$	Estimated	
Cdc20 reactivation	$\overline{\gamma}$	$0.005s^{-1}$	Estimated	
BubR1-Cdc20 dissociation	$\overline{\beta}^c$	$0.001s^{-1}$	Estimated	
APC/C-MCC spontaneous dissociation	$\overline{\alpha}^*$	$0.0001s^{-1}$	In vitro measurement	[24]
MCC-p31 dissociation	$\overline{\alpha}^p$	$25s^{-1}$	In vitro measurement	[14]
APC/C-Cdc20 dissociation	$\overline{\alpha}^c$	$0.005s^{-1}$	In vitro measurement	[20]
Cytoplasmic amplification	μ_{amp}	$0.00001s^{-1}nM^{-2}$	In silico estimate	
Securin degradation	λ	$0.0005s^{-1}nM^{-1}$	In silico estimate	
Mad2 total concentration	m_{TOT}	$100nM$	In vitro measurement	[10]
Cdc20 total concentration	c_{TOT}	$120nM$	In vitro measurement	[10]
BubR1 total concentration	b_{TOT}	$120nM$	In vitro measurement	[10.11]
p31 total concentration	p_{TOT}	$200nM$	In vitro measurement	[15]
APC/C total concentration	a_{TOT}	$80nM$	In vitro measurement	[10,11]
Kinetochore-region radius	R_K	$10nm$	Literature value	[33,34]
Cell model radius	R_C	$9\mu m$	Literature value	[35]

Table 3: The canonical parameters values.

5 Results

Chapter summary:

Utilizing the theory, methodologies, preliminary results and discussions from the previous chapters, the capabilities of the different wait-anaphase signal models are investigated by a series of in silico experiments. It is found that the complex wait-anaphase signal where both MCC and p31 is produced at the unattached kinetochores best can provide the system with the required functionality. Improved performance based on other mechanisms are not identified, but can not be excluded. In general, the models display high sensitivity to small parameter perturbations.*

5.1 Analytical results

5.1.1 Dimensionless reaction diffusion equation

The main motivation to develop a physico-chemical modeling framework of the mitotic checkpoint has been to provide a platform for numerical simulations. The biological models presented in Ch. 2 define a system of 15 molecular species and the same number of partial differential equations (30)-(44). Attempting to solve a system of partial differential equations this size merely analytically is usually not rewarding. However, some insight into the underlying dynamics of the mitotic checkpoint can be obtained by considering the scaling of the differential equations.

Recall from (11) the general reaction-diffusion equation

$$\frac{\partial \vec{u}}{\partial t} = D\Delta\vec{u} + \vec{R},$$

where $\vec{u}$ is a vector of concentration functions. For every molecular component u_i, the reaction-term R_i describes either a first-order forward mass-action reaction,

$$R_i = \pm\eta s_1 s_2,$$

where η have units $(s \cdot nM)^{-1}$ and s_1 and s_2 are substrate concentrations, or a first-order reverse reaction,

$$q = \mp\overline{\eta}\, p\,,$$

where $\overline{\eta}$ have units s^{-1} and p is a protein complex concentration. All concentrations have units *nM*.

Dimensionless time t', length r' and concentration ρ' is defined by

$$t = t'T\,,\ r = r'L \text{ and } \rho = \rho' C\,. \tag{55}$$

Substituting (55) these into (11) yields

$$\frac{C}{T}\frac{\partial \vec{u}'}{\partial t'} = \frac{C}{L^2} D\Delta' \vec{u}' + C\vec{R}'\,,$$

which can be simplified to

$$\frac{\partial \vec{u}'}{\partial t'} = \frac{T}{L^2} D\Delta' \vec{u}' + T\vec{R}'\,, \tag{56}$$

where Δ' is the Laplace operator with respect to r'. Equation (56) can be regarded as the dimensionless reaction-diffusion equation.

In a similar fashion can the dimensionless boundary condition be expressed in terms of the dimensionless flux density j',

$$-\frac{CD}{L}\frac{\partial \vec{u}'}{\partial \vec{n}'} = \frac{CL^3}{4\pi TL^2} j'\,,$$

which simplifies to

$$-\frac{\partial \vec{u}'}{\partial \vec{n}'} = \frac{L^2}{4\pi TD} j'\,. \tag{57}$$

5.1.2 Spatial gradients

In the dimensionless equation (56), the non-dimensional diffusion constant D'

$$D' = \frac{T}{L^2} D$$

can be chosen equal to one.

By matching T to a time scale (there are several) of the cytoplasmic mass action reactions, the length scale of spatial gradients can be calculated by

$$L^C = \sqrt{TD}\,.$$

First, by considering the slowest diffusing molecular species and assuming that they are involved in the fastest reactions in the biological models, i.e., with affinity $25nM$, the smallest characteristic length of the system becomes[1]

$$L^C_{min} = \sqrt{0.04s \cdot 1\mu m^2 s^{-1}} \approx 0.2\mu m = 200nm\,.$$

L^C_{min} is approximately the diameter of the kinetochore. The largest characteristic length is calculated from the fasted diffusing molecules and the slowest reactions,

$$L^C_{max} = \sqrt{10000s \cdot 18\mu m^2 s^{-1}} \approx 424\mu m,$$

which is about 25 cell diameters.

$L^C_{\min}$ and $L^C_{\max}$ defines the theoretical range of characteristic lengths of spatial gradients, considering the extreme time-scales that appear in the cytoplasmic system. However, further analysis indicates that spatial gradients smaller then a few cell radii will not appear in the solutions of the reaction-diffusion equations. The reason is that the molecular species involved in the lowest affinity interactions, which are the fastest, are also involved in higher affinity interactions. The second fastest reaction in the system is a 5000-fold higher affinity reaction than the fastest reaction. A lower range limit that is more descriptive of the spatial

[1] Association rates are assumed to be $1\ s^{-1}nM^{-1}$ (diffusion limited). The affinity is therefore proportional to the dissociation rate in the reaction. The time scale is defined as the invert of the dissociation rate.

gradients that are expected to appear in the system is found by using the second fastest reaction rate of the system, which is the APC/C-Cdc20 interaction with affinity $0.005nM$,

$$L_{min}^{C} = \sqrt{200s \cdot 1\mu m^2 s^{-1}} \approx 14\mu m .$$

L_{min}^{C} corresponds to the approximately 1.5 cell radii.

These results indicate that the characteristic length scales that are expected to appear in the cytoplasmic system are larger than the radius of the cell. The concentration functions are, therefore, almost uniform in the cytoplasm [16], which implies that the system is well mixed. It can therefore be concluded that APC/C activation and Securin degradation occurs simultaneously throughout the cell. Hence, further analysis can be focused on the spatial-mean concentrations of the system, without danger of loosing important spatial information.

The characteristic lengths obtained from the boundary conditions are found assuming the dimensionless flux density in (57) equal to one and matching the time-scale to the kinetochore turnover rate:

$$L = \sqrt{\frac{4\pi TD}{k'}},$$

where k' is the non-dimensionalized constant defined in (47). Considering the slowest and fastest turnover rate at the kinetochore, the characteristic length scales of the spatial gradients near the kinetochore are calculated to be

$$L_{\min}^{K} = \sqrt{4\pi \cdot 100s \cdot 1\mu m^2 s^{-1} \cdot 1.661^{-1} \cdot 10^{-9}} \approx 1nm$$

and

$$L_{\max}^{K} = \sqrt{4\pi \cdot 500s \cdot 18\mu m^2 s^{-1} \cdot 1.661^{-1} \cdot 10^{-9}} \approx 8nm.$$

Both the lower and upper ranges of characteristic length scales near the kinetochore are small compared to the radius of the cell. Spatial gradients are, therefore, expected to be large around the kinetochore region.

From analyzing the scaling of the equations that govern the concentration function both in the cytoplasm and near kinetochores, it can be concluded that spatial gradients are significant in a thin layer around the kinetochore, due to the kinetochore turn over processes, but that

the gradients are flattened at small distances into the cytoplasm. Therefore, the system is said to be well mixed, at least at some small distance away form the kinetochore. In a biological setting, this indicates that, despite the small size of the kinetochore, the intra-cellular distances does not directly pose a challenge for the mitotic checkpoint, since diffusion constants are large enough to carry the wait-anaphase signal across the cell rapidly (Figure 12).

5.1.3 Critique of the reaction-diffusion model

It has been argued that since the solutions of the reaction-diffusion system display almost uniform protein concentration in the spatial dimension, a better approach would be to represent the biological models by a system of ordinary differential equations that describe the reactions, but excludes diffusion [16]. However, such a modeling approach would imply that the central kinetochore turnover rate of MCC, p31* and Cdc20* could no longer be directly connected to boundary flux parameters in the model. The modeling efforts presented in this text intends to stay as close to the actual biological system as possible, something that is partially obtained by including the directly observable measures of the cellular system as parameters in the mathematical models. In such, representing the kinetochore turnover as a flux over the kinetochore-region is strongly preferable, something that can not be obtained in a system of ordinary differential equations. The partial differential equation formulation of the mathematical models is therefore sustained.

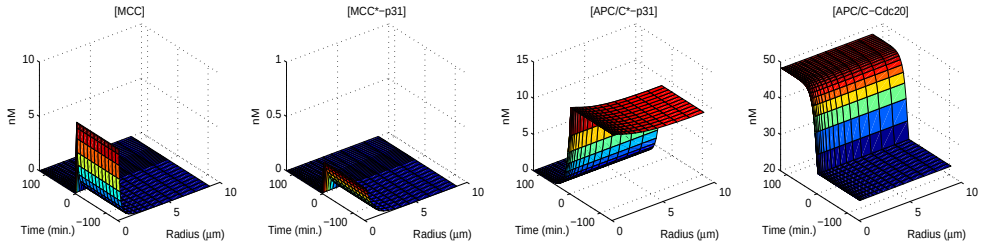

Figure 12: Plots of selected concentrations functions that are parts of a solution of the reaction-diffusion system. Time zero indicates complete kinetochore attachment. The surfaces display steep gradients near the kinetochore-region ($r=R_K$), but is flat elsewhere. This demonstrates that the emitted protein species are quickly transported across the cytoplasm by diffusion. Following complete kinetochore attachment ($t=0$) the spatial gradients vanish, since the kinetochore flux is silenced.

5.2 Evaluation of the core-circuitry

5.2.1 Balancing MCC production and degradation

As commented in Ch. 2.1.3, the core-circuitry is not expected to solely provide both tight inhibition and rapid release, since the observed production rate of MCC is insufficient to balance the needed degradation rate of APC/C-MCC. Therefore, it is proposed that the core-circuitry is accompanied by at least one additional pathway, where cytoplasmic MCC amplification, cytoplasmic MCC assembly and APC/C-MCC lifetime regulation by a complex signal are models currently under investigation.

Prior to testing the potential contributions to the core-circuitry by additional pathways, it is important to consider the conditions under which the core-circuitry could solely be functional. In particular, it should be investigated if the failure of the core-circuitry can be explained by measurement errors in the biological assays used to assess the MCC-production rate. Measurement errors in biology are normally quite large; values within the order of magnitude can often be acceptable. It cannot be ruled out that the measured MCC production rate is an under-estimate and that the real rate is actually higher. If a reasonable enhanced MCC-production rate can provide the core-circuitry with the ability to support both thigh inhibition and rapid release, the role of additional pathways must be reconsidered.

The dissociation rate of APC/C-MCC is constrained by the putative degradation time of approximately 10 minutes (Ch. 2.1.4). Assuming that APC/C-MCC decays as a single exponential, the APC/C-MCC degradation rate can be estimated to

$$\frac{ln2}{10 \cdot 60s} = 0.0012s^{-1},$$

which is an estimate that corresponds closely with the measured value of $0.0013s^{-1}$ [16,38]. Assuming that the estimated APC/C-MCC dissociation rate is accurate, the question becomes what the single kinetochore MCC production rate must be to maintain APC/C-MCC levels. An estimate of the number of MCC-molecules that must be produced at the kinetochore for the core-circuitry to balance the cytoplasmic degradation of can be found by multiplying the dissociation rate of ACP/C-MCC with the total number of APC/C molecules in the system,

$$\mu_{est} = 0.0012s^{-1} \cdot 400000 \approx 500s^{-1}.$$

This suggests that a 5-fold increase in MCC-production would provide a sufficient checkpoint

solely based on the core-circuitry, which is within the under-estimation error that can occur in the assays used. Therefore, based on the above, it cannot be concluded that additional pathways are needed to support tight inhibition and rapid release.

This analysis is based on a rough estimate of single exponential (i.e., single component) decay of APC/C-MCC, after MCC production is silenced. However, the full model includes a much more extensive interaction network, which is likely to make a non-trivial impact of the rate at which the MCC-inhibtion is degraded. Therefore, the above analysis is only good for a first estimate of the MCC-production rate that is needed for the core-circuitry to be functional without additional pathways.

5.2.2 Enhanced MCC production

The failure of the core-circuitry can be further illustrated by a simulation of the mathematical model of the core-circuitry, with parameter values as given in Table 3 (Figure 13a). With one kinetochore emitting the simple MCC-containing wait-anaphase signal, inhibition of APC/C-Cdc20 is poor, with over *30nM* present at steady-sate, before complete kinetochore attachment. This results in complete degradation of Securin before all chromosomes are attachment to the spindle and a failed mitotic checkpoint.

The rough estimate of what MCC production rate that is needed to balance the degradation of the inhibited APC/C suggests that a 5-fold enhancement of the measured value should provide a successful checkpoint. This is confirmed by a simulation, which provided 97% inhibition and a release time of 11 minutes (Figure 13b).

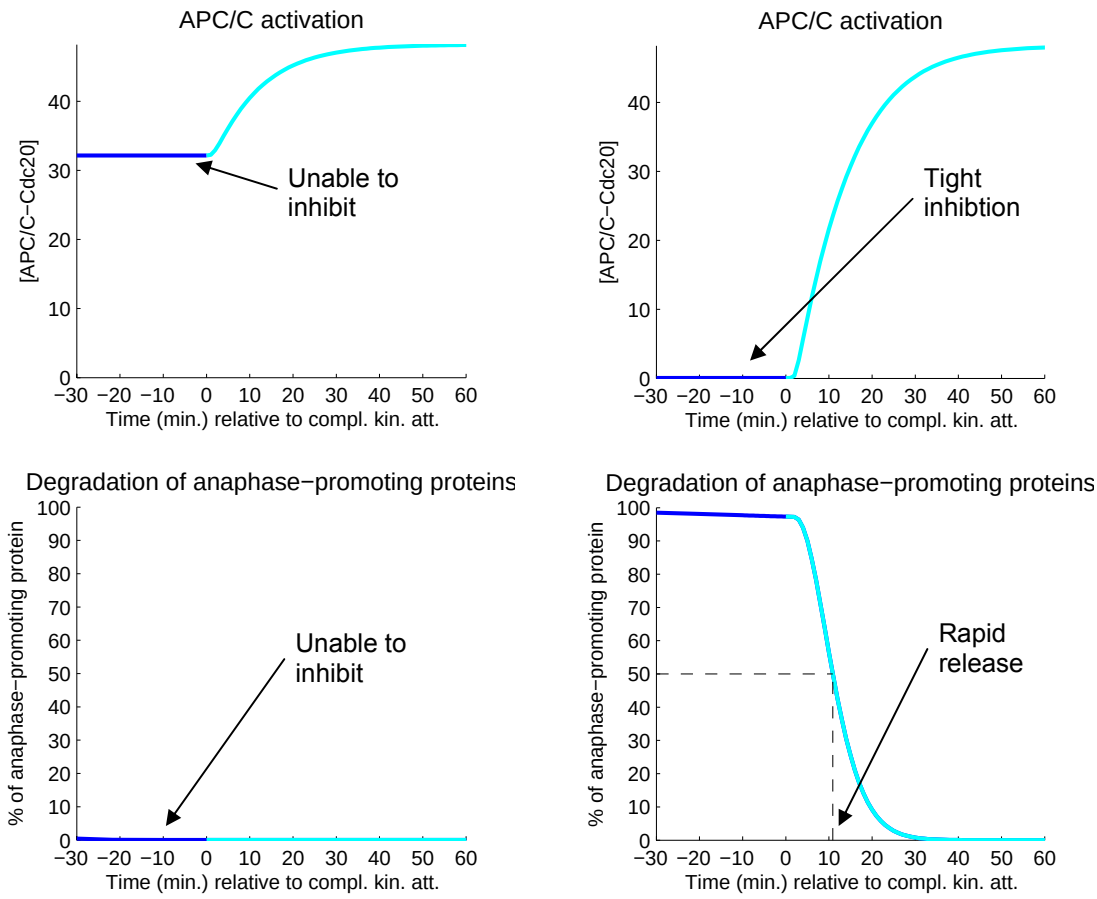

Figure 13a (left) and 13b (right): The left panels demonstrates the failure of the core-circuitry model, with a single kinetochore MCC production rate equal the measured value (100 molecules per second). At the time of complete kinetochore attachment, active APC/C-Cdc20 is present at a concentration of more the *30nM,* something that cause premature Securin degradation. The right panels show the same plot for a simulation with a 5-fold enhancement of the MCC production rate (500 molecules per second). In this simulation the APC/C-Cdc20 level is preserved at 97% at the time of complete kinetochore attachment. The black dotted line indicates that Securin is degraded to 50% of the initial level 11 minutes after complete kinetochore attachment. The concentration functions are colored dark blue before and light blue after the time of complete kinetochore attachment.

To obtain a more nuanced picture of the effect of enhanced MCC-production, the core-circuitry model can be simulated systematically, with variable values of the MCC production rate. This approach can determine at what level an enhancement in MCC production can provide a successful core-circuitry model. An in silico experiment is designed where the kinetochore turnover rate μ is modulated and the degradation of Securin is monitored, together with the release time after complete kinetochore attachment (Figure 14).

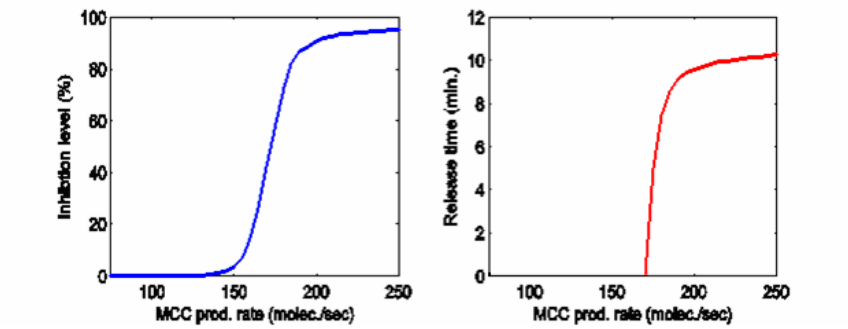

Figure 14: The inhibition level (left panel) is determined by the percentage of the initial level of Securin that is not degraded at the time of complete kinetochore attachment. Per definition, tight inhibition is said to be obtained if 90% or more of the Secruin is preserved at this time, which is the case for a MCC-production rate of 220 molecules per second or more. The release time is defined as the time after complete kinetochore attachment where the Securin level is reduced to 50% (right panel, see also dotted line in Figure 13b). The release time is not defined if the inhibition level is lower then 50% at the time of complete kinetochore attachment. For a proper mitotic checkpoint function, i.e., tight inhibition and rapid release, the inhibition level must be 90% or higher and the release time lower then 30 minutes.

From the results of this in silico experiment it can be concluded that a 2-3-fold increase of MCC-production rate over the measured value is sufficient to provide both tight inhibition and rapid release, strengthening further the conclusion from Ch. 5.2.1 that the failure of the core-circuitry can be explained by a measurement error.

5.2.3 Identifying sensitive parameters in the core-circuitry model

The in silico experiment presented in Ch. 5.2.2 investigates the ability of the system to provide a functional mitotic checkpoint with an enhanced MCC production rate, by simulating the core-circuitry with an increasing rate of MCC production. The parameter μ was highlighted as an obvious candidate that could be modified to provide the system with the ability to tightly inhibit and rapidly release, something that was confirmed by simulation. However, it is not obvious that μ is the only parameter that has this ability. More generally, a similar analysis of all the parameters in the model can be carried out, by simulating the core-circuitry with parameter values both lower and higher then the canonical set, while monitoring the performance of the system. This approach is commonly referred to as a sensitivity analysis, at least in a parameter estimation setting where the structural identifiability of a regression model is of interest [39]. Here, a reaction-diffusion model, built directly from physical and chemical insight of the system, with measured or otherwise a priori determined parameter values, is considered. The structure of such models is defined by the molecular components and interactions that are included. Nevertheless, performing a

sensitivity analysis is useful to investigate which parameters that are critical to the performance of the mitotic checkpoint.

The sensitivity analysis is carried out by modulating all the parameters in the core-circuitry model in a range of 0.01 to 100 times the canonical values. An exception to this modulation range is applied to the geometrical parameters, i.e. cell and kinetochore size, which are varied in a range of *50-300 nm* and *7-15μm,* respectively. The range of geometrical parameters cover the values expected to appear in most normal sized mammalian cells [33,34,35], but do not cover small eukaryotes such as yeast. A total of four reaction parameters are indicated to have the ability to provide the system with tight inhibition and rapid release when modified. The analysis suggests that a MCC production rate enhanced by 2-3-fold over the measured value can provide the system with tight inhibition and rapid release, consistent with the finding in Ch. 5.2.2. In addition, a lowered p31 concentration to approximately 30% of the canonical value can provide tight inhibition; however, the release time suffers from this modification. Similar results are found for a 3-fold increase[2] of the Mad2-p31 affinity or decreased APC/C-MCC-p31 dissociation rate to 30% of the canonical value (Figure 15).

The similarity in the results when modifying the parameters of the p31 catalysis pathway is not surprising, since these modifications all cause an increased catalytic effect. Repression of p31 concentration will naturally contribute to less p31 activity; likewise will a higher Mad2-p31 affinity contribute to a less effective production of the intermediate complex APC/C-MCC-p31, while a low APC/C-MCC-p31 dissociation rate will contribute to slow decay of the concentration of this intermediate complex. In fact, the sensitivity analysis point out all the steps in the p31 catalysis pathways as candidates to provide the system with tight inhibition. On the other hand, the modifications in p31-related parameters result in questionable ability to provide rapid release.

[2] A high affinity interaction is characterized by low ratio between dissociation rate and association rate. In is this ratio that is perturbed in the sensitivity analysis.

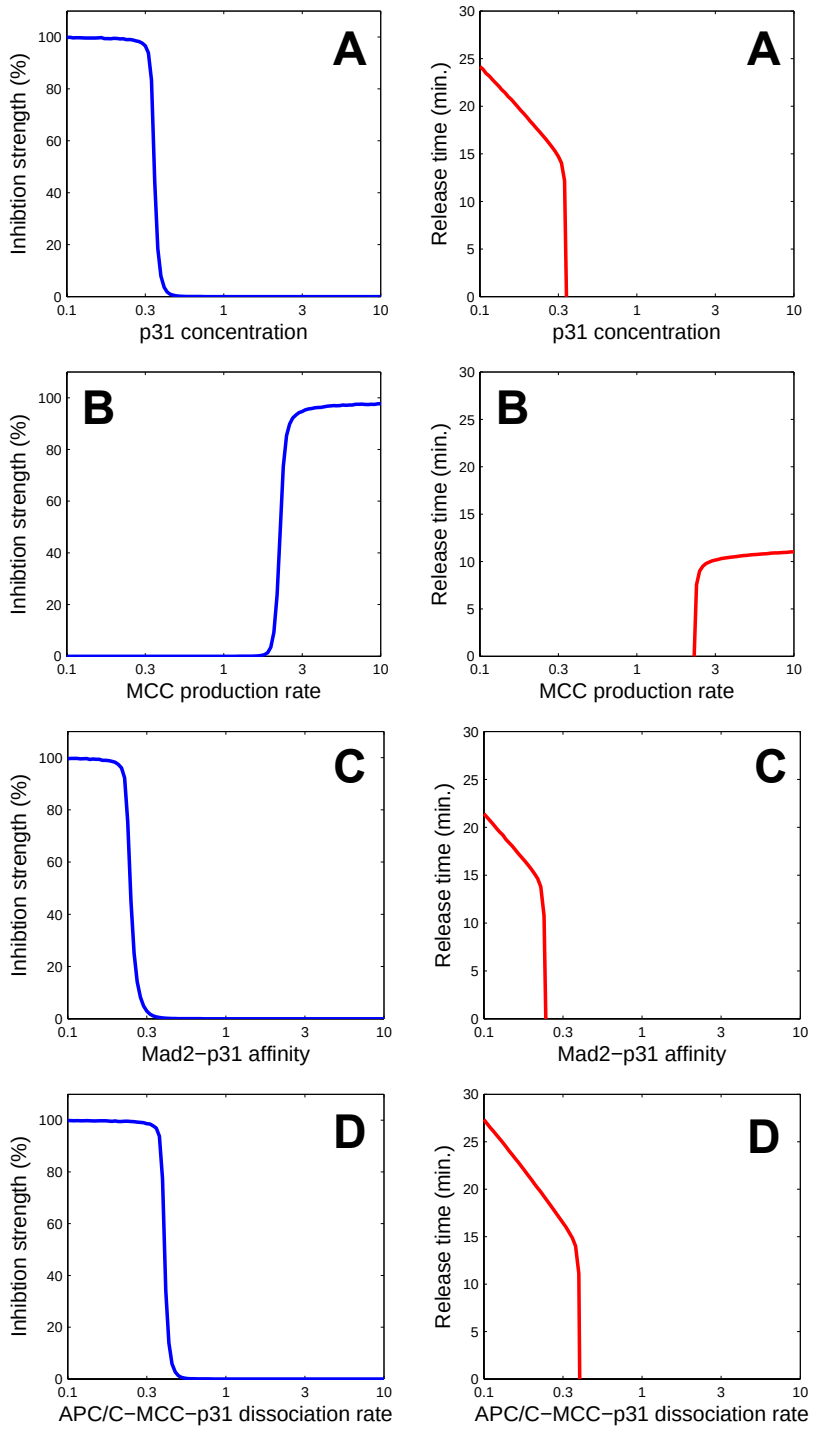

Figure 15: A decrease of p31 concentration level to about 30% of the canonical value provide the system with the ability to tightly inhibit, however, at the cost of a steep increase in release time (A). An enhancement in the MCC production rate provides both tight inhibition and rapid release (see Ch. 5.2.2) (B). An increase in Mad2-p31 affinity (C) and a lowered APC/C-MCC-p31 dissociation rate (D) display similar results as a repressed p31 concentration. This similarity is caused by the unidirectional effects on the modification to the p31 catalytic pathway.

5.2.4 Robustness to system noise in the core-circuitry

The sensitivity analysis in Ch. 5.2.3 revealed that the core-circuitry can provide the mitotic checkpoint system with both tight inhibition and rapid release, assumed an enhanced MCC production rate over the measured value. For this reason, it is not clear that additional pathways are needed for the system to obtain a functional checkpoint.

Any biological system must be able to function properly under the parameter variations that occur naturally within the system or in its surroundings. Protein concentrations in cells within a single cell-line can have a coefficient of variation (CoV)[3] as high as 20% [40]. In addition are the size of the kinetochore and the size of the cell expected to be distributed within a cell line with similar variability [33,34,35]. Reaction rates and diffusion constants, on the other hand, are expected to be constant from one cell to another, since the physical properties that determined these parameters, such as cytoplasmic density, should not change in genetically identical cells.

Supplementary to testing if the core-circuitry can provide tight inhibition and rapid release it is, therefore, interesting to stress the system with noise in protein levels and cell and kinetochore size, in the following denoted as "system noise". The system noise resistance is tested in silico by adding normally distributed white noise at levels of 2, 5, 10 and 20 % CoV to a large number of simulations and monitoring the fraction of these that display both tight inhibition and rapid release. This fraction, called the success rate, is interpreted as a measure of the robustness of the system (Table 4). Already at 5% CoV in system noise is the core-circuitry showing a significant drop in success rate. With 20% CoV in system noise the success rate is 46 %, which can be acceptable at high a noise-level; however, the rapid decay in success rate as a function of system noise is a destructive quality for a biological system. The core-circuitry can therefore not be regarded as sufficiently robust to system noise.

CoV (%)	2	5	10	20
Success rate	1	0.65	0.5	0.46

Table 4: System noise was added to the core-circuitry model at levels of 2, 5, 10 and 20 % CoV (*N=1000*) and the number of simulations that were successful in terms of displaying tight inhibition and rapid release was counted. A simulation was determined to be successful if the Securin level was at 90% or more of the initial value at the time of complete kinetochore attachments and that the Securin level was degraded to 50% within 30 minutes thereafter. The success rate is the fraction of the simulation that maintained both features.

[3] The coefficient of variation is defined as the ratio of the variance and the mean, and is, therefore, a measure of normalized variability.

5.3 Evaluation of the cytoplasmic MCC amplification model

5.3.1 The amplification parameter is hyper-sensitive

In the core-circuitry model, the measured MCC production is too low to balance the observed degradation rate. One possibility is that the measured MCC production rate is an under-estimate due to a measurement error and that the system, in fact, is able to provide both key features needed for a functional checkpoint. However, if the latter is the case, the mitotic checkpoint might not be robust to system noise, as indicated in Ch. 5.2.4. Despite that the MCC production hypothetically can be sufficient for the system to obtain tight inhibition and rapid release, considering other possibilities is motivated by the fact that the core-circuitry seems fragile to disturbances in model parameters, something that a biological system is typically not.

Cytoplasmic amplification has been suggested as an attractive mechanism that can produce MCC away from kinetochores and provide the system with tighter inhibition (see Ch. 2.2) and potentially more robustness to system noise. The amplification is thought to be driven by a conformational change of Mad2, making the MCC capable of mimicking the kinetochore binding sites.

The biological model of the amplification step (Ch. 2.2.2) describes the process by a single bulk parameter, μ_{amp}. No direct measurement is available for this parameter, so an in silico estimate is provided. By investigating a large span of possible values, keeping all other parameters constant according to Table 3, a rough indication of what parameter values that could provide appropriate amplification can be found. For values of μ_{amp} smaller than $10^{-6}\, s^{-1} nM^{-2}$, adding cytoplasmic amplification to the core-circuitry model has virtually no effect. The lower bound of the amplification parameter is, therefore, set to this value. Starting at the lower bound, μ_{amp} is increased gradually, while the temporal APC/C-Cdc20 concentration is monitored. The results indicate that increased amplification increases the ability to inhibit, without disturbing the release time significantly, until a critical value of μ_{amp} is reached. A small increase of μ_{amp} above the critical value provides tight inhibition, but an unfortunate side effect is that the system is not able to release from the inhibited state after complete kinetochore attachment (Figure 16). This unfortunate behavior is explained by the fact that the MCC, after exceeding some threshold concentration, auto-amplifies in an irreversible process. When MCC is auto-amplifying the tight inhibition is unaltered by complete kinetochore attachment. This "hyper-sensitivity" makes the system unable to advantage from the cytoplasmic amplification model, since rapid release is a key feature of a functional mitotic checkpoint.

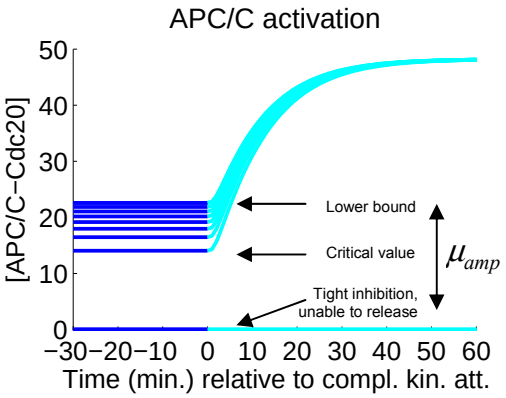

Figure 16: APC/C-Cdc20 spatial mean concentrations for simulations with increasing cytoplasmic amplification strength are plotted. The simulation corresponding to the "lower bound" of μ_{amp} is virtually identical to a simulation of the core-circuitry, i.e., with no amplification mechanism. From the lower bound, the amplification strength is gradually increased with even increments until a critical value is reached. Increasing the amplification strength above the critical value provides tight inhibition, but makes the system unable to release.

5.3.2 Counteraction of the hyper-sensitivity

A possible solution to the problem of hyper-sensitivity in the amplification mechanism is that p31 can balance the amplification by formation of MCC-p31, since this complex can be assumed to have inactivated the binding site that drives the further formation of MCC [14]. Assuming that p31 can balance cytoplasmic MCC amplification, the level of counteraction can be controlled by modulating the concentration of p31 directly. To investigate what combinations of p31 concentration and μ_{amp} that can provide a functional checkpoint, an in silico experiment was carried out by simulating the cytoplasmic amplification model with p31 levels and μ_{amp} values ranging on a log-scale from 0.01 to 100 times the canonical p31 concentration value and the critical value of μ_{amp} (Figure 17).

Another candidate parameter that can potentially be modified to counteract the amplification is the affinity of the MCC-p31 interaction. A similar experiment with modified values of $\overline{\alpha}^{p}$ and μ_{amp} produced almost identical results as displayed in Figure 17 (data not shown).

The experiments failed to identify a counteraction mechanism that is able to balance the hyper-sensitivity of cytoplasmic amplification. Based on this negative result, it is concluded that the cytoplasmic amplification model cannot be underlying the mitotic checkpoint.

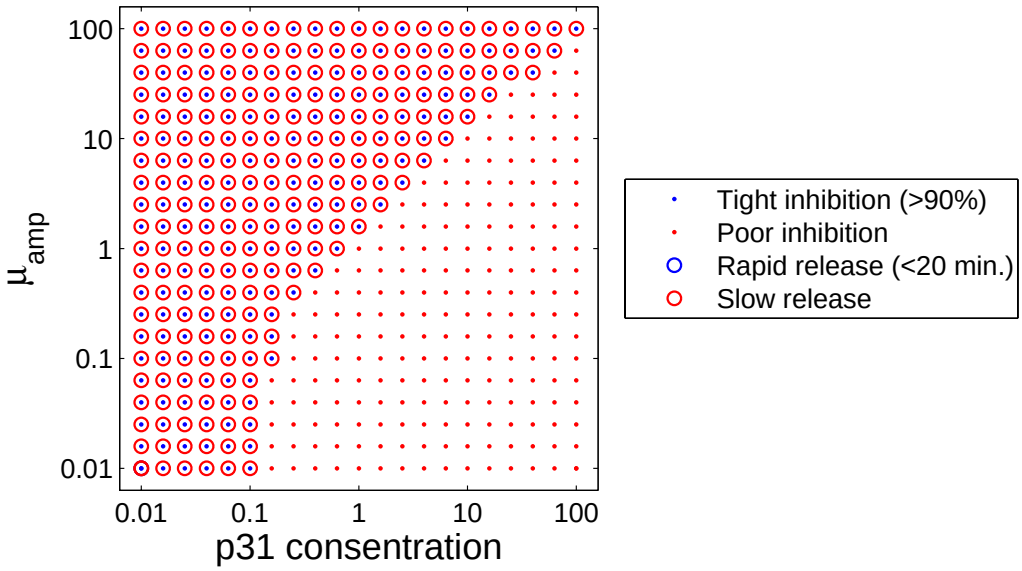

Figure 17: An in silico experiment to test if p31 can counteract the hyper-sensitivity of cytoplasmic amplification. If such counteraction was possible, it would be indicated by a blue dot encapsulated in a blue circle, which does not appear in the graph. In the plot, the log-scaled axes indicate a multiplicative modification from the canonical p31 concentration and the critical μ_{amp} value.

5.4 Evaluation of the cytoplasmic MCC assembly model

5.4.1 Adding MCC assembly to the core-circuitry is destructive

As an alternative to the MCC amplification model, it is suggested that the MCC is assembled in the cytoplasm and that the role of the kinetochore merely is to activate the complex. This model might represent an easier task for the kinetochore than what is posed in the core-circuitry. However, simulations indicate that adding cytoplasmic MCC assembly to the core-circuitry has only a minor effect on inhibition strength and cannot support tight inhibition, at least not with the canonical parameters (Figure 18).

As in the case of the core-circuitry, the possibility of large measurement errors make it hard to conclude steadfastly based on simulations using the canonical values only. A sensitivity analysis was therefore performed to investigate if a modification to any of the parameters could provide a functional system. The results indicate that none of the parameters have this ability (data not shown) and it is be concluded that cytoplasmic assembly model is unlikely to

be underlying the mitotic checkpoint in mammalian cells. The model underperforms in comparison to the core-circuitry, which was indicated to be successful with an enhanced MCC production rate. The MCC assembly model, however, is unsuccessful also after kinetochore capacity enhancement. The explanation lies in the formation of the inactive MCC in the cytoplasm, an interaction that compete APC/C for Cdc20.

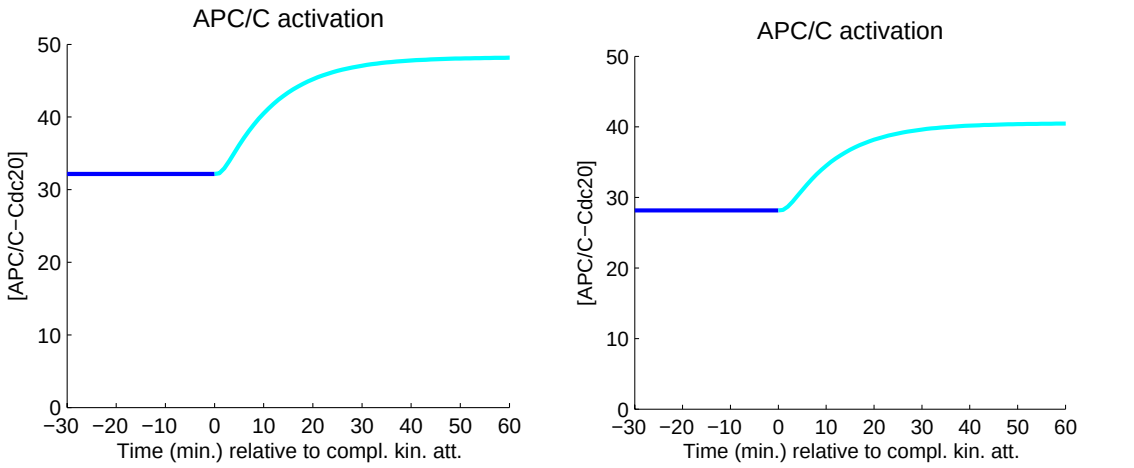

Figure 18: The core-circuitry (left panel) is unable to provide tight inhibition with canonical parameter values. Adding the cytoplasmic MCC assembly model only contributes with a slight increase in the ability to inhibit (right panel).

5.4.2 Cytoplasmic MCC assembly in yeast

The cytoplasmic MCC assembly model was suggested based on the observation that mutated yeast cells can produce MCC without the presence of functional kinetochores (Ch. 2.3.1). A yeast cell is typically only one tenth of a mammalian cell in radius. A test of the validity of the MCC assembly model for yeast is not included in the sensitivity analysis, since the yeast cell radius is outside the modulation range. However, a separate in silico experiment, where the cytoplasmic assembly model is simulated for geometrical parameters taken from yeast data, indicated that the cytoplasmic assembly model can provide tight inhibition and rapid release in yeast (data not shown). In addition, the same ability was tested for the core-circuitry operating solely, an experiment that also displayed a positive result (data not shown). Based on these results, the MCC assembly model can not be rejected in the case of yeast cells, nor can it be concluded to have a significant advantage over the sole core-circuitry model.

5.5 *Evaluation of the complex wait-anaphase model*

5.5.1 Activating the inhibitor, inhibiting the activator

The third suggested mechanism that potentially can provide the mitotic checkpoint with desired features, is the complex wait-anaphase signal model (see Ch. 2.4). This model does, unlike the cytoplasmic amplification and the cytoplasmic assembly models, not rely on a direct modification of the MCC inhibition pathway, but instead on an extension of the p31-pathway. Recall that the role of p31 is to catalyze the disassembly of the inhibited APC/C-MCC-complex and that p31, in such, is a promoter of checkpoint release. Live cell measurements have indicated that p31 turns over at unattached kinetochores (Figure 9), in parallel to MCC production. This turnover is hypothesized to represents production of an inactive state called p31*. Thus, in the complex wait-anaphase model the kinetochore is both activating the inhibitor (MCC) and inhibiting the activator (p31) of anaphase onset.

After the silencing of the dual kinetochore turnover, a decrease in cytoplasmic MCC concentration occurs, together with an increase in cytoplasmic p31 concentration (Figure 19). A simulation of the core-circuitry with canonical parameters, added p31* turnover at the unattached kinetochores, demonstrates that these two transitions together makes the system more potent to tightly inhibit the APC/C-Cdc20 complex, as well as rapidly reactive when kinetochore attachments are completed (Figure 20).

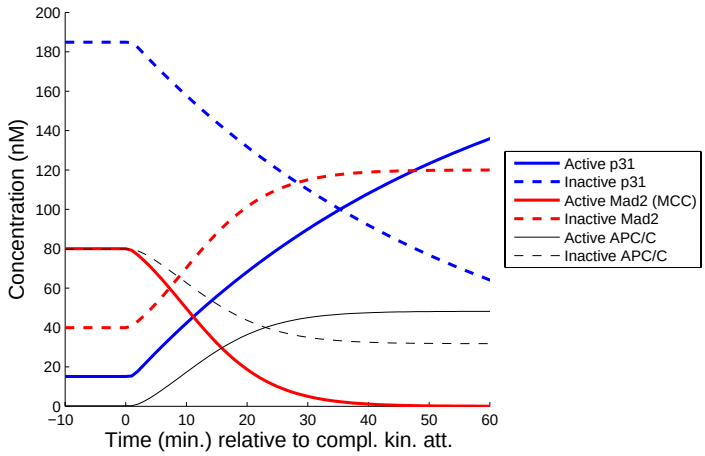

Figure 19: The complex wait-anaphase signal produces a double switch in protein concentration following complete kinetochore attachment. The anaphase inhibitor (MCC) is present at approximately *80nM* prior to attachment and drops to zero after (red line). The anaphase promoter (p31) is repressed to below *20nM* prior to attachment, and increases after the final attachment is made (blue line). A high steady-state concentration of the inhibitor and a repressed concentration of the promoter can provide tight inhibition of APC/C (black line). Following complete kinetochore attachment (*t=0*) a double switch, i.e., from active to inactive anaphase inhibitor (red+dotted lines) and from inactive to active anaphase promoter (blue+dotted lines), result in rapid anaphase onset (see Figure 20).

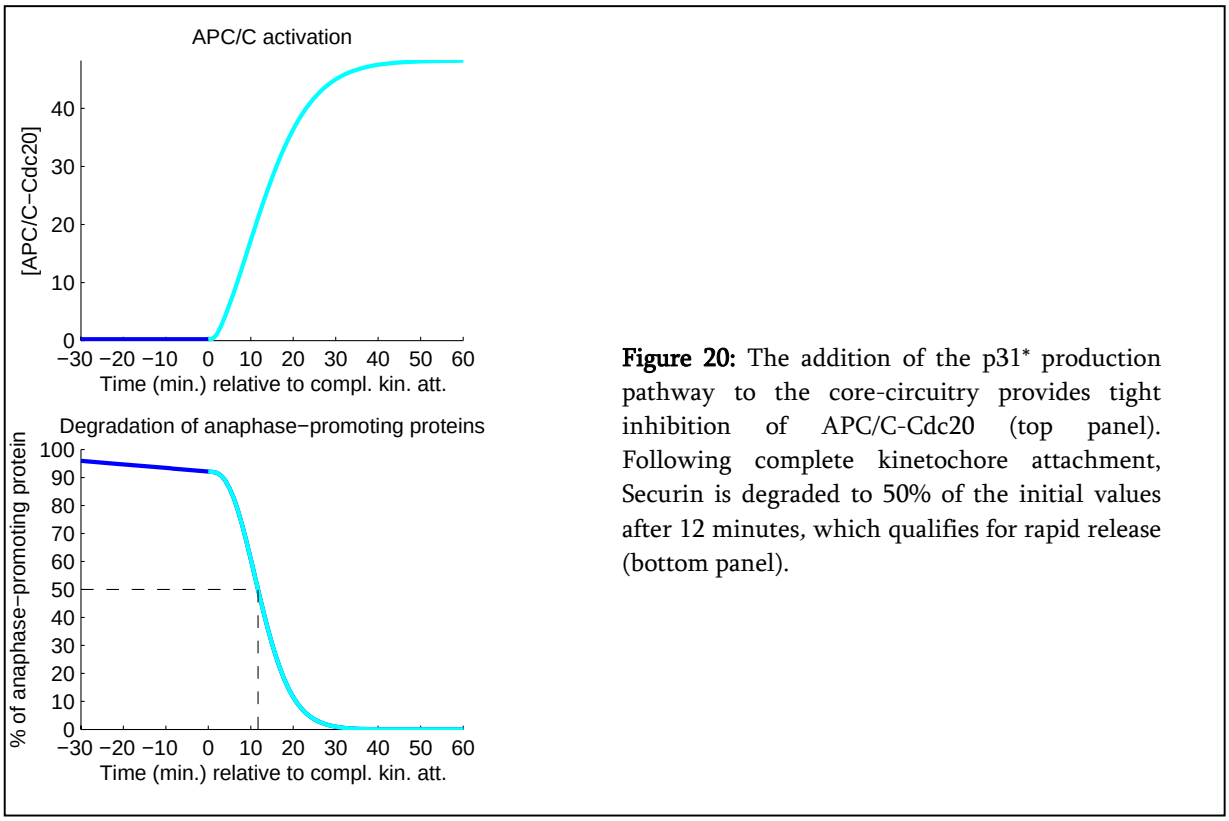

Figure 20: The addition of the p31* production pathway to the core-circuitry provides tight inhibition of APC/C-Cdc20 (top panel). Following complete kinetochore attachment, Securin is degraded to 50% of the initial values after 12 minutes, which qualifies for rapid release (bottom panel).

5.5.2 Identifying sensitive parameters in the complex wait-anaphase model

In the case of the cytoplasmic MCC amplification and assembly models, both unsuccessful with the canonical parameter set, the interpretation when sensitive parameters were discovered was that a measurement error potentially can explain the lack of tight inhibition and rapid release. For the complex wait-anaphase signal model, which is successful, sensitive parameters can potentially lead to false conclusions, since a measurement error can provide the desired functionality based on favorably measured, but not real, parameter values. In addition, if a highly sensitive parameter is under natural variation in the biological system (i.e., system noise), it is clear that these parameters must be under strict regulation by some intrinsic mechanisms to avoid that the system becomes fragile.

The sensitivity analysis of the complex wait-anaphase signal indicates that several parameters are highly sensitive, even to small perturbations of the parameters. Most remarkable is the sensitivity result of Cdc20 concentration, which rapidly causes lack of inhibition both when up- and down-regulated (Figure 21). Based on this result it can be concluded that even a small perturbation of the Cdc20 concentration level from the measured value, either in terms of system noise or a measurement error, will cause a serious disfunctionality of the mitotic checkpoint. This finding is consistent with recent reports [25], which suggest that Cdc20-

levels must be strictly regulated for proper mitotic checkpoint functionality. A molecular mechanism that potentially can reduce the sensitivity of the Cdc20 concentration parameter is suggested in Ch. 2.5, but the implication of this model is treated separately in Ch. 5.7.

Further are all parameters that regulate the p31 catalysis pathway sensitive to perturbations that cause an increase in APC/C-MCC degradation rate. Most obviously, increasing p31 concentration is immediately causing decreased inhibition strength. Likewise will a decreased p31* production rate or an increased p31* reactivation rate cause a decrease in inhibition strength. The interactions that cause the catalytic effect of p31 on APC/C-MCC disassembly are regulated by the Mad2-p31 affinity and the spontaneous dissociation rate of APC/C-MCC-p31, which both are sensitive to up-regulation in terms of maintaining tight inhibition (Figure 22).

The three next parameters that are indicated to be sensitive in the analysis are the MCC-components Mad2 and BubR1 and the MCC production rate. Down-regulation of the latter will, obviously, result in a weaker MCC-inhibtion of the APC/C. Likewise will removal of the components Mad2 and BubR1 have a similar effect (Figure 23). APC/C-Cdc20 affinity, spontaneous MCC disassembly rate, BubR1-Cdc20 affinity and APC/C-Mad2 affinity are indicated to be less sensitive than the parameters discussed above, but can cause problems, both in terms of inhibition and release (Figure 24). Diffusion constant and the geometric parameters are insensitive (data not shown).

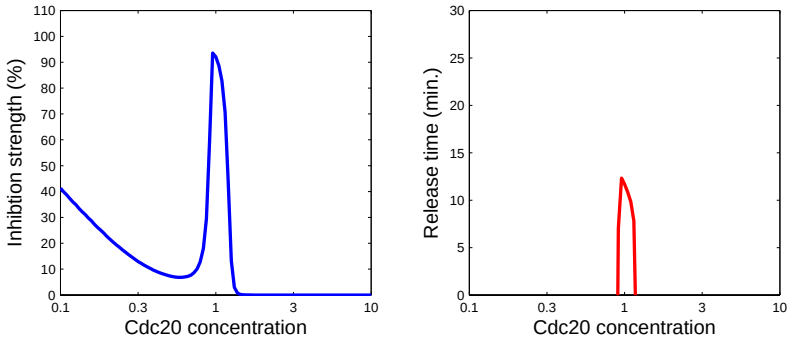

Figure 21: The Cdc20 concentration levels is a highly sensitive parameter, and cause lack of inhibition both when up- and down-regulated. The dual sensitivity can be explained by the fact that Cdc20 is both a component in the MCC (inhibitor) and, by it self, the activator of the APC/C.

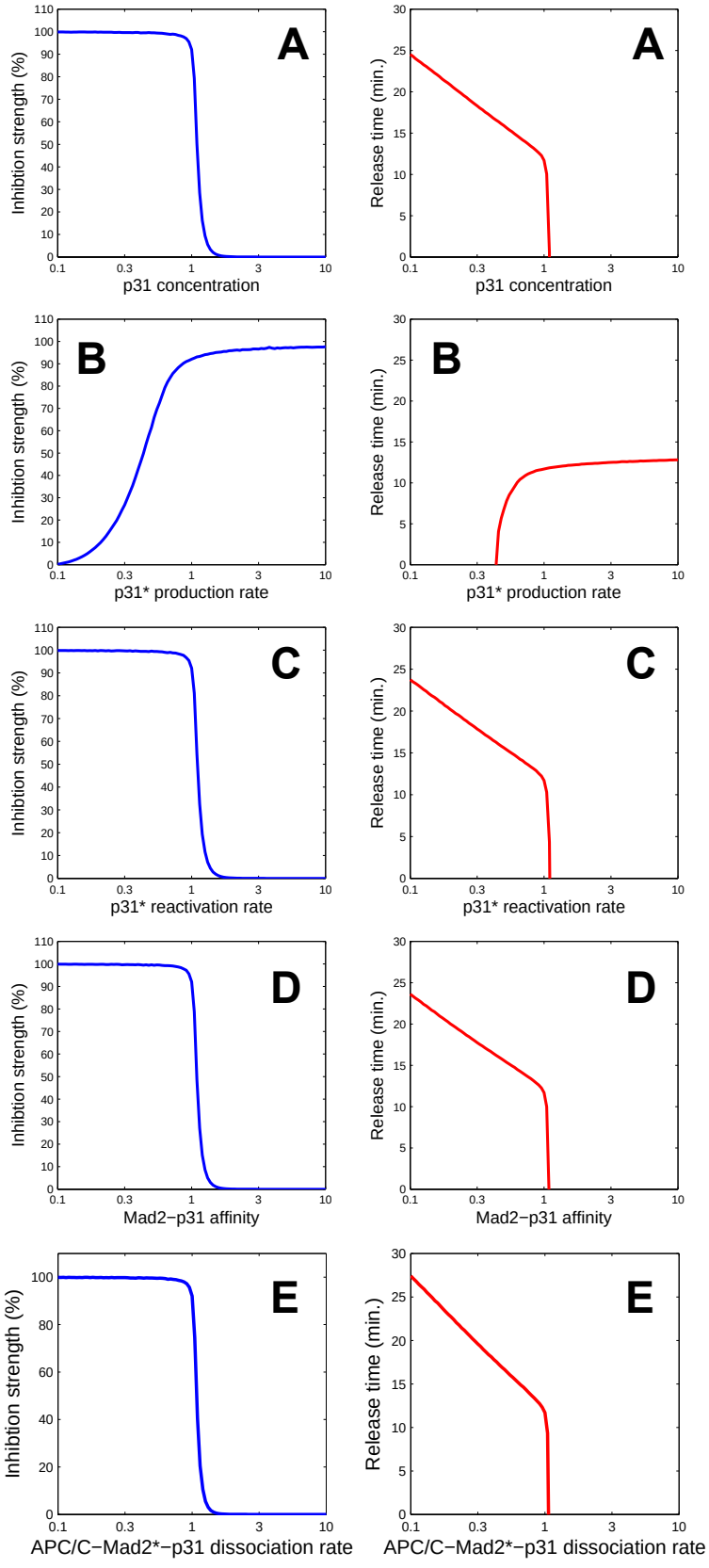

Figure 22: All parameters involved in regulating the p31 interactions with the MCC pathway are sensitive to modulation in a single direction. Up-regulation of p31 causes a faster destruction of the MCC assembly and altered inhibition strength (A). A similar effect is observed if the p31* production rate is decreased or if the p31* reactivation rate is increased, something that cause more active p31 in the cytoplasm (B and C). A lower Mad2-p31 affinity or higher APC/C-MCC-p31 dissociation rate allows faster relaxation of the MCC-inhibtion, which also alters the inhibition strength (D and E).

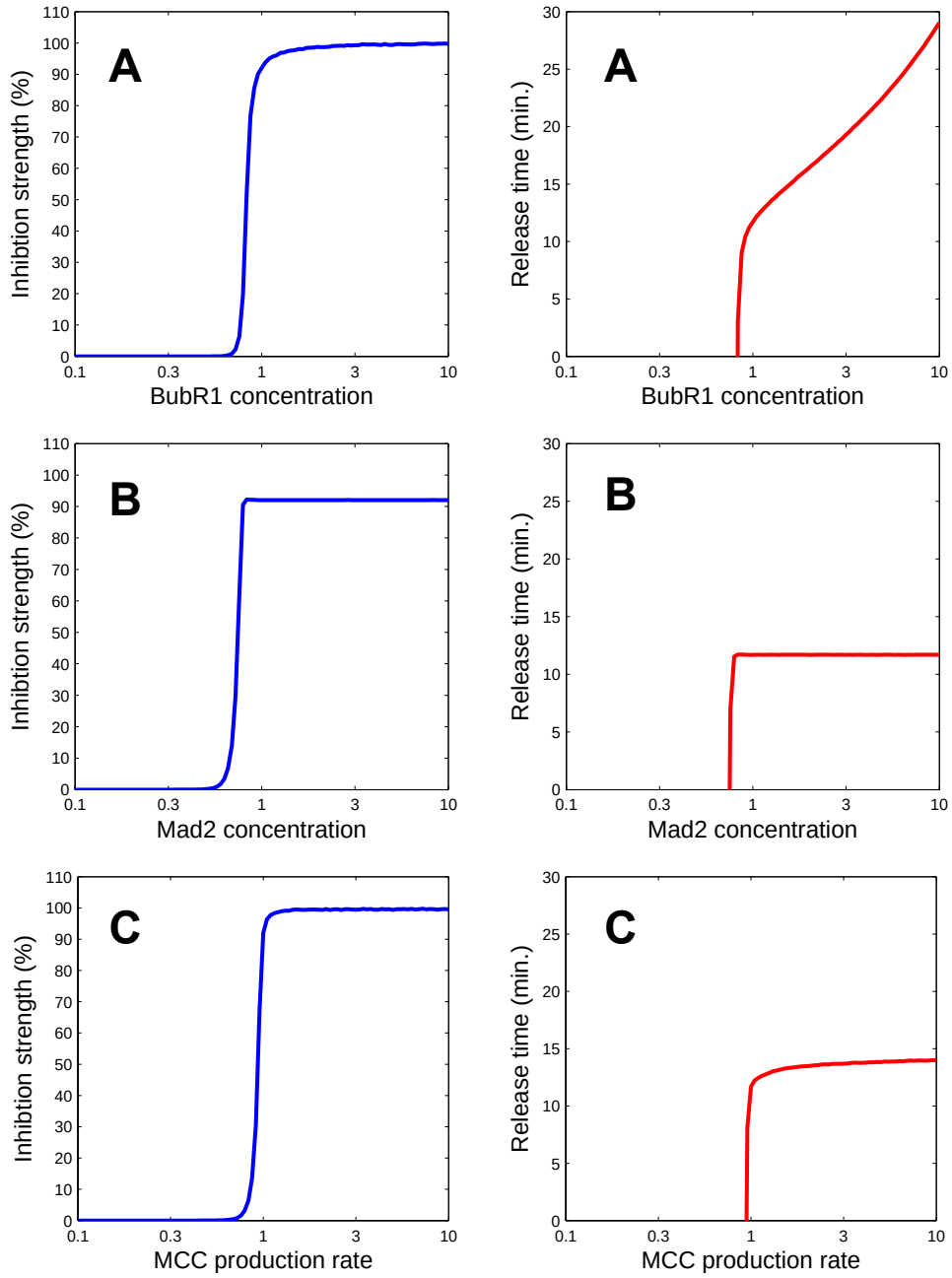

Figure 23: The concentration of the MCC-components Mad2 and BubR1 are both sensitive to down-regulation, since lack of these components hinder sufficient formation of the inhibiting complex (A and B). Similarly, decreasing the MCC production rate alters the ability to inhibit APC/C activation (C).

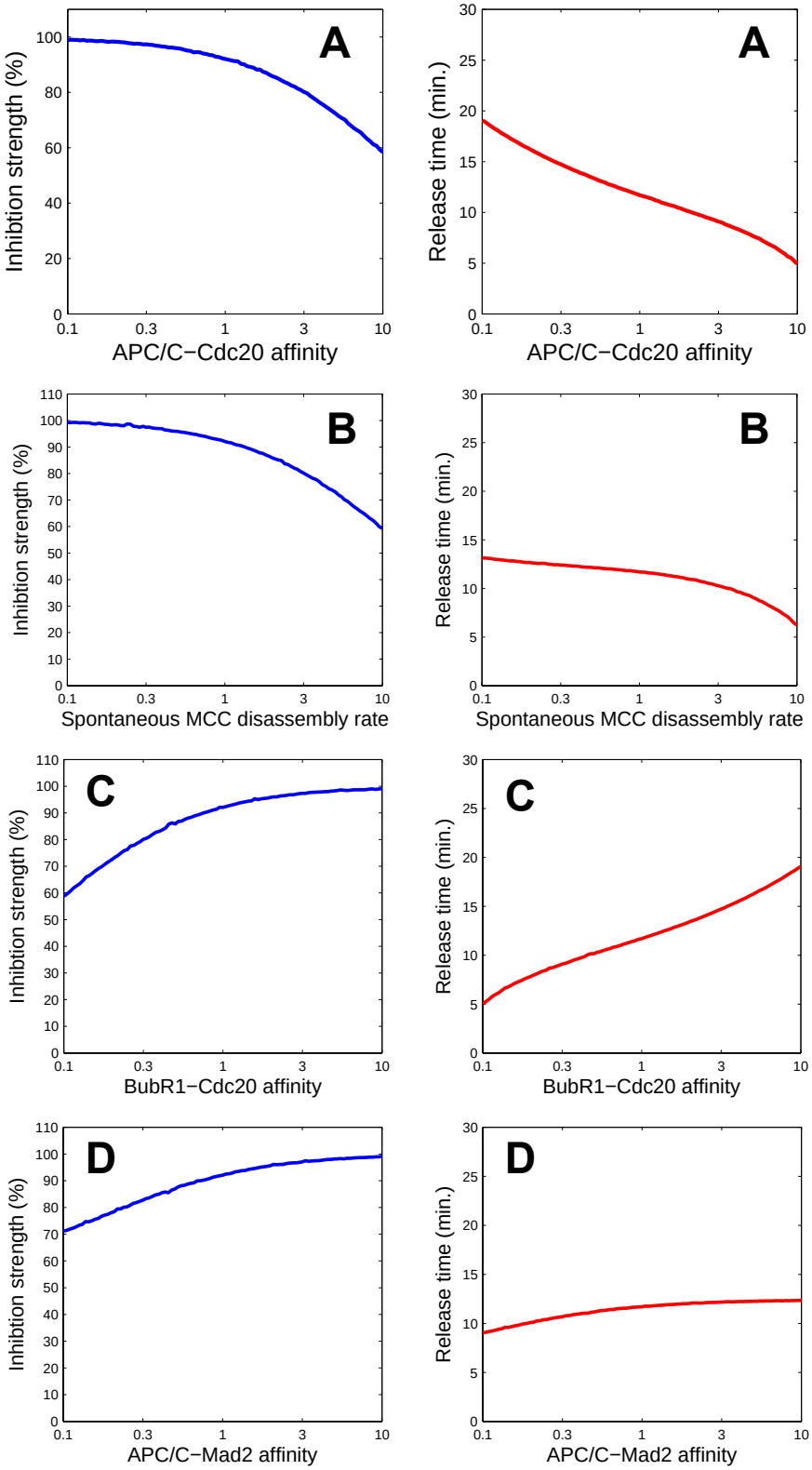

Figure 24: APC/C-Cdc20 affinity (A), spontaneous MCC disassembly rate (B), BubR1-Cdc20 affinity (C) and APC/C-Mad2 affinity (D) are intermediately sensitive.

5.5.3 Robustness to system noise in the complex wait-anaphase model

The capacity of the complex wait-anaphase model to function under system noise can be tested in silico by an experiment identical to that presented in Ch. 5.2.4 (Table 5). In comparison to the corresponding results of the enhanced MCC production model, the complex wait-anaphase signal display a significant increase in ability to resist system noise, particularly at small CoV-levels (Figure 25).

CoV (%)	2	5	10	20
Success rate	1	1	0.76	0.55

Table 5: System noise was added to the complex wait-anaphase model in a similar fashion as in the robustness analysis of the core-circuitry (*N=1000*). Robustness data from both models are presented in Figure 25.

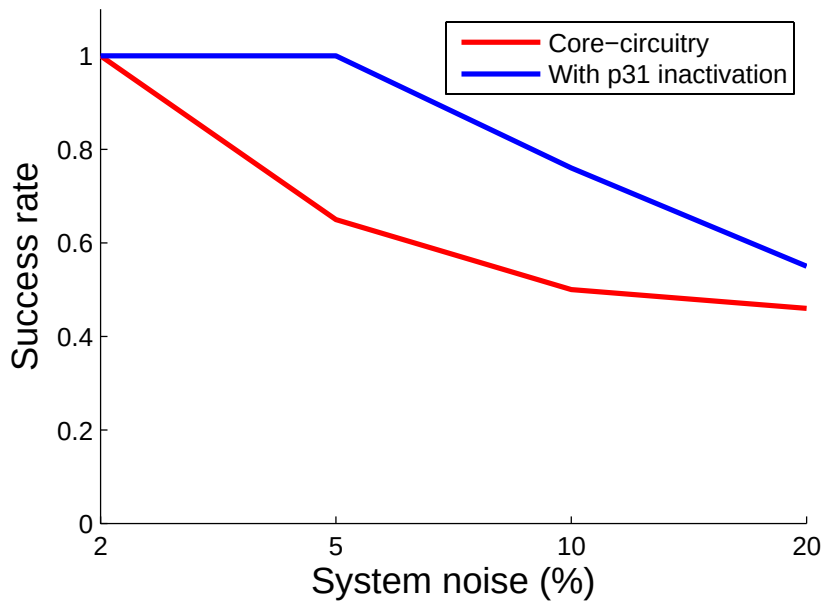

Figure 25: The robustness of the core-circuitry (Table 4) (red line) plotted in comparison to robustness data obtained from simulations (*N=1000*) of the complex wait-anaphase model (Table 5) (blue line). Adding p31* production makes the mitotic checkpoint more viable to resist system noise than the sole core-circuitry.

The x-axis in not in scale.

5.6 Model combinations

5.6.1 Models do not exclude each other

Neither of the biological models suggested to provide the mitotic checkpoint with tight inhibition and rapid release exclude the other models. Despite the negative results obtained when testing if cytoplasmic amplification and assembly can support a functional checkpoint, it is unclear if either of these models can play a role in combination with one of the other models. Thus, the models should also be tested in combinations.

5.6.2 Performance matrix

The three suggested models span the upper half of a 3-by-3 matrix of combinations (Table 6). The diagonal entries are the models by them selves and are thoroughly tested in Ch. 5.3-5.5. This leaves three model combinations to be investigated further.

Cytoplasmic MCC amplification result in hyper-sensitivity when combined with both cytoplasmic assembly and p31* production. Therefore, the conclusion that the cytoplasmic amplification model cannot be underlying the mitotic checkpoint is sustained. The combination of p31* production at kinetochores and cytoplasmic MCC assembly is able to tightly inhibit and rapidly release (data not shown). The molecular interactions that suggested these two models are discovered independently of each other. In fact, the protein species p31 is not a component of the yeast system [36], while cytoplasmic MCC assembly is observed exclusively in yeast. Because of the different origin of the models, the relevance of the success of this combination is not clear. Taken that it is relevant, it is still unknown if the success arise as a consequence of a synergetic effect or if merely the introduction of the p31*-pathway lowers the requirements of MCC production so that the before insufficient cytoplasmic assembly pathway now appears as a feasible option.

Cyt. amp.	Cyt. ass.	p31* prod.	
Able to inhibit, but not release (hyper-sensitive).	Able to inhibit, but not release (hyper-sensitive).	Able to inhibit, but not release (hyper-sensitive).	Cyt. amp.
	Not able to inhibit.	Able to tightly inhibit and rapidly release.	Cyt. ass.
		Able to tightly inhibit and rapidly release.	p31* prod.

Table 6: The three model combinations displayed in matrix form. Model behavior description in red text indicates failure, while green indicates success.

5.7 Cdc20 buffering

5.7.1 Sensitivity of Cdc20 concentration

The sensitivity analysis of the complex, p31*-producing, wait-anaphase model indicates that the concentration of Cdc20 is particularly sensitive to both up- and down-regulation (Figure 21). A sensitivity analysis of the core-circuitry with enhanced MCC production, which is a successful model in terms of tight inhibition and rapid release, display similar results (data not shown). This indicates that the sharp peak that appears in the sensitivity analysis of the Cdc20 concentration parameter should be regarded as a general property of the core-circuitry, and not be associated particularly to the addition of the p31*-pathway.

Because of the small range of Cdc20 concentration that the mitotic checkpoint models can function within, noise in the Cdc20 concentration component is probably causing more lack of resistance to system noise than other parameters. In a recent report [25], a buffering of excess Cdc20 is suggested as a mechanism that can provide enhanced robustness to temporal fluctuations in protein levels. There is no immediate link between the temporal and cell-to-cell protein variation phenomena; however, the suggested temporal regulation has motivated the hypothesis that Cdc20 turnover at kinetochores (Ch. 2.5) serves as a mechanism that buffers system noise.

In the biological models, the level of active Cdc20 in the cytoplasm is regulated by an inactivating mechanism at the kinetochores. A single kinetochore is thought to turn over approximately 500 Cdc20 molecules per second, in parallel to MCC- and p31*-production. For the case of human cells there are 46 chromosomes and twice as many kinetochores. Because the Cdc20 turnover is independent of the attachment state of the kinetochores, the total Cdc20* production can therefore be as large as 50000 molecules per second around the time of complete kinetochore attachment.

The mathematical modeling framework is constructed around the turnover of a single kinetochore, while Cdc20* is produced by every kinetochore. Based on the fact that all kinetochores in a cell receives substrate from a larger cytoplasmic volume than a single kinetochore does, it can be assumed that the substrate limitations that are effecting the MCC- and p31*-pathways does not apply for the Cdc20*-pathway. The Cdc20* production therefore fall in between a kinetochore-bound and a cytoplasmic event. Simulating the Cdc20* production merely as a last unattached kinetochore turnover process, cannot support a capacity of 50000 molecules per second, since diffusion is too slow to provide sufficient substrate. To see the effect of Cdc20 buffering, the Cdc20 turnover is, therefore, modeled in part as a cytoplasmic event in this in silico experiment.

5.7.2 Buffering of Cdc20 enhance model robustness

To investigate if production of Cdc20* at all kinetochores can produce a less sensitive system, the wait-anaphase model can be simulated for various Cdc20 concentrations and Cdc20* production rates. Starting at the canonical parameter set and performing repeated sensitivity analyses with increasing Cdc20 buffering levels reveals a clear reduction in sensitivity to up-regulation of Cdc20 concentration (Figure 26).

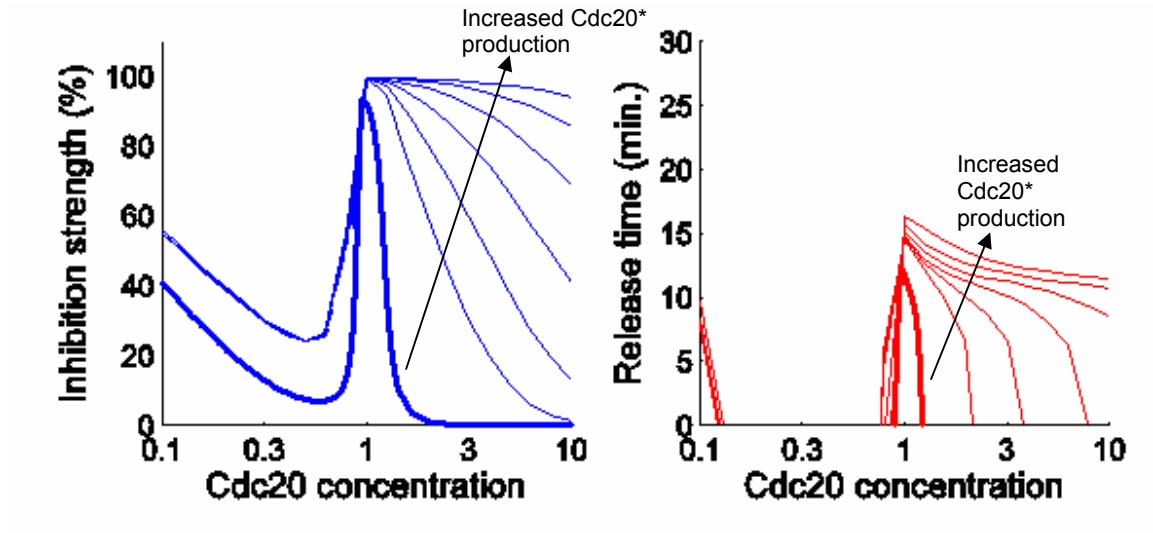

Figure 26: A simulation with canonical parameters display a sharp peak in Cdc20 concentration sensitivity (think lines). To investigate the effect of Cdc20 buffering, the sensitivity analysis was repeated with increasing Cdc20* production rates (along the arrows), resulting in a widening of the sensitivity peak.

6 Discussion, conclusions, and future work

Chapter summary:

Biophysical and statistical limitations of the mathematical modeling approach are discussed, before conclusions are drawn about the nature of the wait-anaphase signal. Finally, future modeling efforts and experiments are suggested.

6.1 Limitations of the mathematical approach

6.1.1 Critical biophysical assumptions

The mathematical models in this text are founded on the assumption that the molecular kinetics of the wait-anaphase signal can be simulated reasonably well by mass-action kinetics and uniform diffusion. Neither is necessarily true.

The protein molecules themselves occupy as much as 40% of the physical space in the cytoplasm. In fact, the cell is so densely filled that modelling cytoplasmic protein as a crystal structure, rather than soluble particles, has been suggested [41]. In addition, the free movement of particles is partially blocked by several solid cytoplasmic structures and membranes. Despite the obvious problems the crowdedness of the cytoplasm can cause for the diffusion model, it is commonly assumed that many protein species move around the cytoplasm by random walks. The diffusion constants applied in this text are measured in vivo, and are therefore thought to represent the true rate of motion in the system. However, it is not clear that the basic diffusion theory applied to accommodate these measurements is appropriate. From normal 3-dimensional diffusion theory it is derived that the mean-square displacement *d* increases linearly in time, such that $\delta = 1$ in the relation

$$\left\langle d^2 \right\rangle = 6Dt^{\delta}.$$

There are several reports of measurements of cytoplasmic diffusion where the assumption that $\delta = 1$ is invalid [42]. A better fit between theory and observation is obtained by introducing the sub-diffusion exponent $\delta < 1$. Unfortunately, a general modelling framework for the reaction-diffusion processes equivalent to the partial differential equation formulation given in Ch. 3.1 does not exist in the case of sub-diffusion [43]. An alternative to deterministic modelling is to incorporate sub-diffusion by simulating the stochastic nature of the molecule movements explicitly; however, such an approach typically demand more computer power than what is available and pose an even harder challenge in assessing model parameters.

The validity of the mass-action assumption is also debatable in an intra-cellular context. In vitro experiments where molecular interactions are tested in strongly non-homogenous media indicate that mass-action reactions fail to describe the observed kinetics. As an alternative to the mass-action assumption, it has been suggested in the literature [44] to model cytoplasmic interactions by fractal-like kinetics, where the constant diffusion-limited rate k is replaced with a time dependent term. For an interaction between molecular species x and y, the association process is then described by

$$\frac{dx}{dt} = \frac{dy}{dt} = -k(t)xy\,,$$

where

$$k(t) = k_0 t^{-\xi}\,,\ \xi \geq 0\,.$$

The parameter ξ is called the fractal parameter and describes the level of heterogeneity in the system. If the system is homogenous, or made homogenous by vigorous stirring, $\xi = 0$ and the theory is in line with classic mass-action kinetics. For $\xi > 0$, fractal-like kinetics incorporate a degradation of reaction rates over time. This degradation is a consequence of the systems lack of ability to remain well mixed, since diffusion is limited. In the mitotic checkpoint system, incorporating a potential disability to remix might play an important role, particularly in terms of the blending of the molecular species produced locally at the kinetochore into the cytoplasm.

Introducing fractal-like kinetics in the wait-anaphase signal model can provide a better description of the biophysical environment expected to be found in the cytoplasm. However, the theory is only immediately applicable for reaction systems, and it is not clear how the theory can be applied in a reaction-diffusion system. For the theory of fractal-like kinetics to

be useful in a reaction-diffusion setting, the parameter k must be specified in the spatial dimension,

$$k = k(\vec{r}, t).$$

If the remixing ability of the system is itself homogenous, k is constant in the spatial dimension and must only be specified as a function of time. If such homogeneity can not be assumed, which might be necessary to capture the spatial differences the theory is set out to capture, a full spatio-temporal specification of k is demanded.

Considering that the model is already starved in terms of measured parameter values, introducing reaction parameters that must be specified in space, time or both does not appear as a desirable option until measurement techniques are in place to match the level of detail already present in the models.

Measurement techniques and computer power, and possible even fractal-reaction-sub-diffusion equations, are expected to advance in the future, something that might provide an opportunity to model intra-cellular signalling networks more realistically. Until, then the established biological models and the available measurements can appropriately be accommodated in mathematical models based on ordinary diffusion and mass-action theory. However, a strict criterion should be that all parameters are in line with measurements or literature values that reflect the observed rates of the system.

6.1.2 Measurement error and system tuning

Among the canonical parameters in Table 3 are 20 of the values obtained by direct measurement, derived from measurements or obtained from the literature, while seven parameters are estimated. Several of the biological assays that have provided the measured values introduce large measurement errors. Therefore, there is a certain degree of freedom present in choosing the canonical values, both in the case of measured and unmeasured parameters. Within the bounds of equally reasonable parameters, the canonical set is identified by optimizing the system performance. The system is therefore to a limited degree tuned to a set of parameter values that provides successful simulations.

If a canonical parameter perturbation that can be explained by measurement or tuning error cause severe performance corruption, the relevance of the models and the conclusions drawn from them becomes questionable. Unfortunately, the results from Ch. 5 indicate that several of the measured parameters are highly sensitive to small perturbations. Most clearly, the sensitivity of Cdc20 concentration in the complex wait-anaphase signal model, before adding

Cdc20 buffering, demonstrates this issue (Figure 21). The sensitivity indicates that system performance is weakened if the level is modified only 10% in either direction, which certainly is within the expected measurement errors and initial tuning of the system.

It is clear that the sensitivity analysis is dependent of the initial choice of canonical values. If a more detailed measurement than that of the current canonical set becomes available and this measurement is outside the functional range, an immediate conclusion might be that the system is dysfunctional. However, it can not be ruled out that there are other errors in the canonical set and that there exist a better choice of canonical parameters that makes the system functional, with the new measurement incorporated. In such, the sensitivity analyses can be misleading, possibly too pessimistic, in terms of judging the system to be sensitive to small perturbations. The reason is that only simulations around a fixed point in the parameter space, i.e., the canonical parameters, are investigated. A better, and more exhausting, strategy would be to test the entire subspace of equally reasonable parameter values for a functional range for each modification. However, this is left for future work.

6.2 How does the wait-anaphase signal work?

6.2.1 Least subset of molecular interactions

Molecular biology is an extremely complex field of science. Mathematical models of intra-cellular signalling networks typically encompass only a fraction of the full set of known interactions that are relevant to a system. In general, if only two molecules are interacting and each can be modified in n and m distinct ways, respectively, the total number of bimolecular interactions is 2^{n+m-2} [45]. Therefore, the number of genuine molecular species that can be products of only a few proteins and their binding partners can easily be several hundred. Thus, a true representation of the actual knowledge about a biological system, i.e., a model where all relevant species and reactions are included, can typically give raise to hundreds of differential equations. Since the number of measurements normally cannot follow the combinatorial explosion in variables and parameters the uncertainty in simulation results soon becomes very large. Therefore, models usually include only the most significant molecular species and reactions. Alternatively can variables and reactions be bulked to reduce the size of models. This type of model reduction can be both necessary and useful in obtaining a quantitative framework that can accommodate the existing measurements. On the other hand, if too little is included in the model, predictive power can not be expected.

The sum of the core-circuitry and one or more of the three suggested additions to it is thought to represent a least subset of molecular interactions that can explain the main behaviour the wait-anaphase signal. Several molecular species that are known to be essential to the mitotic checkpoint are left out of the models. The rationale behind these exclusions is that the roles of the molecules are complementary to included species in terms of describing the dynamics of the system. For example is the Mad1 protein not included, but accounted for implicitly, since Mad1 is active in the mitotic checkpoint when bound to Mad2. Several reaction rates as also in bulk. The most apparent example is the cytoplasmic MCC amplification parameter μ_{amp}, which represents the mimicking of the kinetochore by the MCC in the cytoplasm, thought to be a multi-step process involving many molecular species.

6.2.2 Conclusions about the wait-anaphase signal

The wait-anaphase models are constructed to capture the main known features of the mitotic checkpoint signalling system. However, it is clear that the models represent only a partial understanding how the entire system actually works. Building a mathematical model of an incomplete system can provide insight into what is unknown, since comparison of simulation results and observed behaviour can suggest what the function of the unknown components ought to be. When investigating biological systems in silico, emphasizing to learn about the unknown parts that are not included in the models are at least of equal importance as obtaining deeper insight into what is already known. In this respect, the following main conclusions can be drawn about the wait-anaphase signal:

- Based on the analysis and simulation of the core-circuitry, it seems unlikely that sole MCC production at kinetochores is the basis of the wait-anaphase signal. The measured MCC production rate might be an under-estimate; still, the core-circuitry will be fragile to system noise.

- The complex wait-anaphase signal model, based on inactivation of p31 at unattached kinetochores, is demonstrated to have the ability to enhance inhibition, release and robustness performance. The rationale behind the success of this model is that it represents a double pathway that both inhibits the promoter and promotes the inhibitor. The turnover at unattached kinetochores of p31 is already demonstrated in living cells; however, the deactivation mechanism is yet to be shown.

- The up-regulation of Mad2 cause cells to have prolonged metaphase arrest [46]. In the wait-anaphase signal models, however, increasing the Mad2 concentration parameters have no effect on the release time (Figure 23). The inconsistency in simulation and observation identifies that the biological models are in lack of an alternative pathway for MCC production, making the simulations incapable of imitating the observed behaviour. This mechanism might correspond to the ability in yeast to produce MCC independently of kinetochores.

- None of the models that were tested in this text display sensitivity results that that are compatible with the level of uncertainty in the canonical parameter set. It cannot be ruled out that the analyses of the models are based on an advantageous, or disadvantageous, canonical parameter set, and that the actual parameters would produce different results and conclusions. The generally high sensitivity displayed in the results might indicate that the models are in lack of important molecular mechanisms.

- The models capabilities to perform under high levels of system noise are not immediately fulfilling the requirement of a high-fidelity system. A cytoplasmic amplification step might play a role in providing enhanced robustness; however, a mechanism that can counteract the auto-amplification after complete kinetochore attachment must be identified.

- Cdc20 concentration is highlighted as highly sensitive parameter, both to up- and down-regulation. The observed independent Cdc20 turnover at kinetochore is demonstrated as a functional mechanism to buffer the over-expression of Cdc20 and partially decrease sensitivity. As in the case of the p31*-pathway, the inactivation mechanism of Cdc20 at kinetochore is not demonstrated.

6.3 Future work and suggested experiments

6.3.1 Future modelling efforts

The models of the wait-anaphase signal describe the concentration of 15 molecular species in space and time. Simulations of a system this size produce a large amount of information and extracting the useful measures is not trivial. In addition, the presence of large uncertainties in many parameter values is troublesome. A simpler, but more focused, model can ease these issues and possibly provide an opportunity to ask more specific questions about certain parts of the system. Therefore, in parallel to expanding the wait-anaphase models as more information becomes available, efforts in the opposite direction, aiming to prune the models to a minimum of essential interactions, is an interesting approach.

The complex wait-anaphase model is demonstrated to enhance system performance, and is therefore highlighted as a candidate for future investigation. A central feature of the complex wait-anaphase model is the dual control of molecular behaviour by the kinetochore, which both inhibits the activator and activates the inhibitor (Ch. 5.5.1). A model focused on the functionality of this dual control can be constructed by incorporating a set of phenomenological components called the “Activator”, the “Inhibitor” and the “Anaphase Promoter” in a reaction-diffusion model. Further, it can be assumed that each component can take two states, namely “on” or “off”. This system is easily illustrated by a 3-dimensional coordinate system, where the axes indicate how large a fraction of the components that are in the different states (Figure 27). From such model one could pursue to define the state of the Anaphase Promoter as a function of the states of Activator and Inhibitor, and hopefully shed more light on under what circumstances the system can perform optimally.

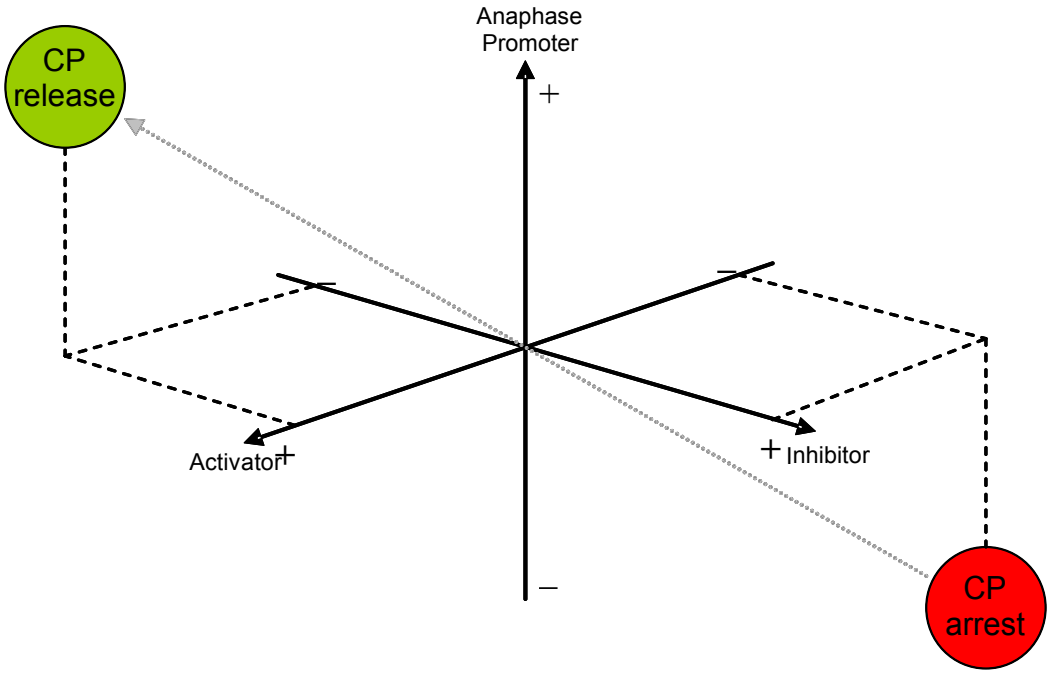

Figure 27: The focused model of the complex wait-anaphase signal can be described as a 3-dimensional coordinate system. The "x-axis" indicates what fraction of the Activator that is in the different states: "on" (+) or "off" (-). The "y-axis" indicates the state of the Inhibitor. When the Inhibitor is on and the Activator is off, the Anaphase promoter, as indicated on the "z-axis", is off and the cell is in mitotic checkpoint arrest. When all kinetochores obtain attachments a change in state in both Activator and Inhibitor to the opposite "sign" causes the rapid onset of the Anaphase promoter and transition from mitotic checkpoint arrest to release (grey arrow).

6.3.2 An unexplainable observation: The two-spindle experiment

In a classic mitotic checkpoint paper, an elegant experiment where fused cells are observed in mitosis is reported [47]. The fused cells have two mitotic spindles and double sets of chromosomes. Surprisingly, the experiment showed that spindles with complete kinetochore attachments entered anaphase regardless of the presence of unattached kinetochores in a neighbouring spindle $20\mu m$ away. This demonstrates that the wait-anaphase signal is unable to communicate throughout the fused cytoplasm that anaphase onset is premature, which is a contradiction to the fundamental assumptions that the signal is diffusible in the entire cytoplasm. The fact that the cytoplasmic content is twice that of a normal cell can be a partial explanation to this issue, since the single kinetochore turnover capacity is not constructed to handle a doubled amount of cytoplasmic protein. However, it is reported that a neighbouring spindle go into anaphase with as many as five signalling kinetochore in close proximity.

A wait-anaphase signal model where the kinetochore-produced molecules are only required to diffuse a short distance before an active transport mechanism, possibly allocated to the mitotic spindle, distributes the signal throughout the cell has been suggested [16]. This would only allow for wait-anaphase signalling within the spindle network; hence, a neighbouring spindle will obey its own mitotic checkpoint unaffected by the surroundings.

The conclusions of the two-spindle experiment do not correspond to the assumption that the wait-anaphase signal is freely diffusible. On the other hand, more recent observations of the wait-anaphase signal components in the cytoplasm indicate that the protein species are diffusible [9,38]. The results that favour an active transport model are relatively old, and current measurement techniques are better suited to provide clear evidence of the nature of the wait-anaphase signal. Since determining if the signal components are diffusible or not is fundamental for the validity of the reaction-diffusion model, it is suggested that the two-spindle experiment is revisited in the future, to provide clearer answers to this question.

6.3.3 Distinct behaviour in APC/C-MCC-p31 concentration

Simulations of the complex wait-anaphase model reveal interesting dynamics in the interaction between p31 and the APC/C-MCC complex. The hypothesized intermediate complex, ACP/C-MCC-p31, is predicted to display a rapid increase in concentration shortly after complete kinetochore attachment, because of the increase in active p31 concentration in the cytoplasm. Subsequently, as the pool of APC/C-MCC is degraded, the concentration of the intermediate complex will fall. Together, this predicts a “bump” in APC/C-MCC-p31 concentration, something that is consistent with simulation results (Figure 28).

A large pool of p31 will display slower diffusion in the period of high APC/C-MCC-p31 concentration, due to the fact that APC/C succeeds p31 in molecular size by almost 100-fold. Observing the dynamics of tagged p31 in a small excitation volume by FCS can detect the expected change in diffusion constant (see Figure 8a for methodology). Observing the hypothesized behaviour of the APC/C-MCC-p31-complex will provide a confirmation that the p31-catalysis pathway is a good representation of the cellular system.

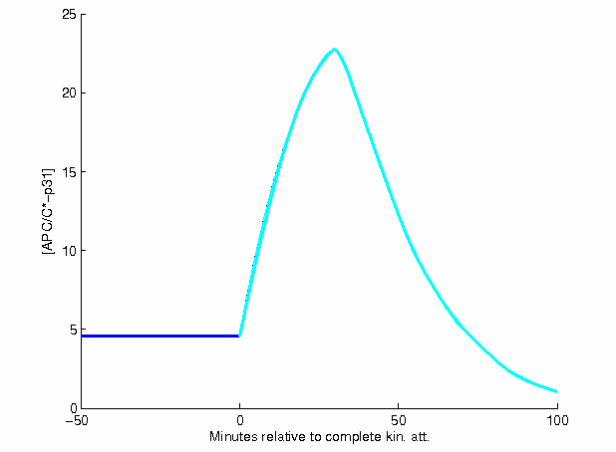

Figure 28: Following complete kinetochore attachment the concentration of the ACP/C-MCC-p31-complex is predicted to increase rapidly to about 5-fold of the steady state value before attachment. The increase lasts for approximately 30 minutes, before the concentration falls towards zero in an exponential fashion. This results in about hour long "bump" in concentration.

References

[1] Alberts, B., et. al. Molecular Biology of the Cell, 4th edition (2002) *Garland Science*.

[2] Morgan, D.O. The Cell Cycle: Principles of Control, 1st edition (2007) *New Science Press Ltd*.

[3] Collins, K., Jacks, T. & Pavletich, P. The cell cycle and cancer (1997) *PNAS* **94**, 2776-2778.

[4] Shah, J.V. & Cleveland, D.W. Waiting for anaphase:Mad2 and the Spindle Assembly Checkpoint (2000) *Cell* **103**, 997-1000.

[5] Rieder, C.L., Cole, R.W., Khodjakov, A., Sluder & G. The Checkpoint Delaying Anaphase in Response to Chromosome Monoorientation (1995) *J Cell Biol* **130**, 941-8.

[6] Musacchio, A. & Hardwick, K.G. The spindle Checkpoint: Structural Insights Into Dynamic Signalling (2002) *Nat Rev Mol Cell Biol* **3**, 731-41.

[7] Hoyt, M.A., Totis, L. & Roberts, B.T. S. cerevisiae genes required for cell cycle arrest in response to loss of microtubule function (1991) *Cell* **66**, 507-17.

[8] Li, R. & Murray, A.W. Feedback control of mitosis in budding yeast (1991) *Cell* **66**, 519-31.

[9] Musacchio A. & Salmon E.D. The spindle-assembly checkpoint in space and time (2007) *Nat Rev Mol Cell Biol* **8(5)**, 379-93.

[10] Sudakin, V., Chan, G.K. & Yen, T.J. Checkpoint inhibition of the APC/C in HeLa cells in mediated by a complex of BUBR1, BUB3, CDC20, and MAD2 (2001) *J Cell Biol* **154**, 925-36.

[11] Tang, Z., Bharadwaj, R., Li, B. & Yu, H. Mad2-Independent Inhibition of APC^{Cdc20} by the Mitotic Checkpoint Protein BubR1 (2001) *Dev Cell* **1**, 227-37.

[12] Habu, T., Kim, S. H., Weinstein J. & Matsumoto, T. Identification of MAD2-binding protein, CMT2, and its role in mitosis (2002) *Embo J* **21**, 6419-28.

[13] Reddy S.K., Rape M., Margansky W.A. & Kirschner M.W. Ubiquitination by the anaphase-promoting complex drives spindle checkpoint inactivation (2007) *Nature* **446(7138)**,921-5.

[14] Mapelli, M., Filipp, F.V., Rancati, G., Massimiliano, L., Nezi, L., Stier, G., Hagan, R.S., Confalonieri, S., Piatti, S., Sattler, M. & Musacchio, A. Determinants of conformational dimerization of Mad2 and its inhibition by p31comet (2006) *Embo J* **25**, 1273-84.

[15] Xia, G., Luo, X., Habu, T., Rizo, J., Matsumoto, T. & Yu, H. Conformation-specific binding of p31comet antagonizes the function of Mad2 in the spindle checkpoint (2004) *Embo J* **23**, 3133-43.

[16] Sear, R.P. & Howard, M. Modeling dual pathways for the metazoan spindle assembly checkpoint (2006) *Proc Natl Acad Sci U S A* **103**, 16758-63.

[17] Shah, J.V., Botvinick, E., Bonday, Z., Furnari, F., Berns, M. & Cleveland, D.W. Dynamics of Centromere and Kinetochore Proteins: Implications for Checkpoint Signalling and Silencing (2004) *Curr Biol* **14**, 942-52.

[18] Howell, B.J., Moree, B. Farrar E.M. Stewart, S., Fang, G. & Salmon, E.D. Spindle Checkpoint Protein Dynamics at the Kinetochore in Living Cell (2004) *Curr Bio* **14**, 953-964.

[19] Stryer, L. Biochemistry, 4th edition (1995) *W.H. Freeman & Company.*

[20] Wang, Z., Shah, J. V., Berns, M. W. & Cleveland, D. W. In vivo quantitative studies of dynamic intracellular processes using fluorescence correlation spectroscopy (2006) *Biophys J* **91**, 343-51.

[21] De Antoni, A., Pearson, C.G., Cimini, D., Canman, J. C., Sala, V., Nezi, L., Mapelli, M., Sironi, L., Faretta, M., Salmon, E.D. & Musacchio, A. The Mad1/Mad2 Complex as a Template for Mad2 Activation in the Spindle Assembly Checkpoint (2005) *Curr Biol* **15**, 214-25.

[22] Poddar, A., Stukenberg, P.T. & Burke, D.J. Two Complexes of Spindle Checkpoint Proteins Containing Cdc20 and Mad2 Assemble during Mitosis Independently of the Kinetochore in Saccharomyces cerevisiae (2005) *Eukaryot Cell* **4**, 867-78.

[23] Kirkeby, H., Manak, M.S., Guan, Y., Brear, A., & Shah, J.V. APC/C Inhibition and Rapid Anaphase Onset Without Cytoplasmic Amplification (2007) *Poster presentation CHROMO2007, under preparation for journal publication.*

[24] Hagen, R. S. Regulation of the Spindle Checkpoint by Mad2 Binding Proteins, PhD Thesis, Dept. of Biology, MIT (2005) *MIT Libraries.*

[25] Doncic, A., Ben-Jacob, E. & Barkai, N. Noise resistance in the spindle assembly checkpoint. (2006) *Mol Syst Biol* **2**, 2006 0027.

[26] Tang, Z., Shu, H., Oncel, D., Chen, S. & Yu, H. Phosphorylation of Cdc20 by Bub1 provides a catalytic mechanism for APC/C inhibition by the spindle checkpoint (2004) *Mol Cell* **16**, 387-97.

[27] Howsion, O.J, S., Lacey, A. & Movchan, A. Applied Partial Differential Equations, revised edition (2003) *Oxford University Press*.

[28] Zumdahl, S.S. Chemical Principals, 3rd edition (1998) *Houghton Mifflin.*

[29] Logan., J.D. An Introduction To Nonlinear Partial Differential Equations (1994), *John Wiley & Sons*

[30] Trotter, H.F. On the Product of Semi-Groups of Operators (1959), *Proc Am Math Soc* **10(4)**, 545-51..

[31] Dill, K.A & Bromberg, S. Molecular Driving Forces: Statistical Thermodynamics in Chemistry and Biology (2007) *Oxford University Press*.

[32] Buffin, E., Emre, D. & Karess, R.E. Flies without a spindle checkpoint (2007) *Nat Cell Biol* **9(5)**, 565-72.

[33] McEwen, B.F., Ding Y. & Heagle A. Relevance of kinetochore size and microtubule-binding capacity for stable chromosome attachment during mitosis in PtK1 cells (1997) *Chrom Research* **6**, 123-32.

[34] Cherry, L.M., Faulkner, A.J, Grossberg, L.A. & Balczon R. Kinetochore size variation in mammalian chromosomes: an image analysis study with evolution implication (1989) *J Cell Sci* **92**, 281-9.

[35] Anderson, E.C. & Petersen, D.F. Cell Growth and Division II. – Experimental Studies of Cell Volume Distributions in Mammalian Suspension Cultures (1967), *Biophys J* **7**, 354-64.

[36] Doncic, A., Ben-Jacob, E. & Barkai, N. Evaluating putative mechanisms of the mitotic spindle checkpoint (2005) *Proc Natl Acad Sci U S A* **102**, 6332-7.

[37] Odde D.J. Chromosome capture: take me to your kinetochore (2005) *Curr Biol* **15(9)**, 828-32.

[38] Shah, J.V., Wang, Z., Kops, G., McLeod, I., Yates, III J. R., Berns, M. W. & Cleveland, D.W. Biochemical composition and cellular dynamics of a mitotic checkpoint complex (2007) *submitted for publication*.

[39] Jaqaman, K. & Danuser, G. Linking data to models: data regression (2006) *Nat Rev* **7**, 813-9.

[40] Sigal, A., Milo, R., Cohen, A., Geva-Zatorsky, N., Klein, Y., Liron, Y., Rosenfeld, N., Danon, T., Perzov, N. & Alon, U. Variability and memory of protein levels in human cells (2006) *Nature* **444(7119)**, 643-6.

[41] Fulton, A.B. How Crowded is the Cytoplasm? (1982) *Cell* **30**, 345-347.

[42] Banks, D.S.& Fradin C. Anomalous Diffusion of Proteins Due to molecular Crowding (2005) *Biophys J* **89** 2960-71.

[43] Schimidt, M.G.W., Sagues F. & Sokolov, I.M. Mesoscopic desciption of reactions for anomalous diffusion: a case study (2007) *J Phys & Cond Mat* **19**,

[44] Schnell, S., Turner T.E. Reaction kinetics in intracellular environments with macromolecular crowding: simulations and rate laws (2004) *Prog Biophys & Mol Bio* **85** 235-60.

[45] Aldright, B.B., Burke, J.M., Douglas, A.L. & Sorger, P.K. Physicochemical Modelling of Cell Signalling Pathways (2006) *Nature Cell Biology* **8(11)**, 1195-1203.

[46] Sotillo, R., Hernando, E., Diaz-Rodriguez, E., Teruya-Feldstein, J., Cordon-Cardo, C., Lowe, S.W. & Beneara R. Mad2 Overexpression Promotes Aneuploidy and Tumorigenesis in Mice (2007) *Cancer Cell* **11**, 1-15.

[47] Rieder, C.L., Khodjakov, A., Paliulis, L.V., Fortier, T.M., Cole, R.W. & Sluder G. Mitotis in Vertebrate Somatic Cells With Two Spindles: Implications for the Metaphase/Anaphase Transition Checkpoint and Cleavage (1997) *Proc Natl Acad Sci USA* **94**, 5107-12.

Figures that are not the authors own works are credited in the text.